การประเมินสมรรถนะของกระบวนการรีฟอร์มมิงแก๊สชีวภาพแบบเคมิคอลลูปปิงที่มีการดูดซับร่วมกับระบบเซลล์เชื้อเพลิงพีอีเอ็มอุณหภูมิสูง

นายศรัณยู เกษมอนันต์

วิทยานิพนธ์นี้เป็นส่วนหนึ่งของการศึกษาตามหลักสูตรปริญญาวิศวกรรมศาสตรมหาบัณฑิต
สาขาวิชาวิศวกรรมเคมี ภาควิชาวิศวกรรมเคมี
คณะวิศวกรรมศาสตร์ จุฬาลงกรณ์มหาวิทยาลัย
ปีการศึกษา 2558

PERFORMANCE ASSESSMENT OF A BIOGAS SORPTION ENHANCED CHEMICAL LOOPING REFORMING PROCESS INTEGRATED WITH HIGH TEMPERATURE PEM FUEL CELL SYSTEM

Mr. Sarunyou Kasemanand

A Thesis Submitted in Partial Fulfillment of the Requirements
for the Degree of Master of Engineering Program in Chemical Engineering
Department of Chemical Engineering
Faculty of Engineering
Chulalongkorn University
Academic Year 2015

Thesis Title	PERFORMANCE ASSESSMENT OF A BIOGAS SORPTION ENHANCED CHEMICAL LOOPING REFORMING PROCESS INTEGRATED WITH HIGH TEMPERATURE PEM FUEL CELL SYSTEM
By	Mr. Sarunyou Kasemanand
Field of Study	Chemical Engineering
Thesis Advisor	Assistant Professor Amornchai Arpornwichanop, D.Eng.

Accepted by the Faculty of Engineering, Chulalongkorn University in Partial Fulfillment of the Requirements for the Master's Degree

.....Dean of the Faculty of Engineering
(Associate Professor Supot Teachavorasinskun, D.Eng.)

THESIS COMMITTEE

.....Chairman
(Associate Professor Soorathep Kheawhom, Ph.D.)
.....Thesis Advisor
(Assistant Professor Amornchai Arpornwichanop, D.Eng.)
.....Examiner
(Pimporn Ponpesh, Ph.D.)
.....External Examiner
(Suthida Authayanun, D.Eng.)

ศรัณยู เกษมอนันต์ : การประเมินสมรรถนะของกระบวนการรีฟอร์มมิงแก๊สชีวภาพแบบเคมิคอลลูปปิงที่มีการดูดซับร่วมกับระบบเซลล์เชื้อเพลิงพีอีเอ็มอุณหภูมิสูง (PERFORMANCE ASSESSMENT OF A BIOGAS SORPTION ENHANCED CHEMICAL LOOPING REFORMING PROCESS INTEGRATED WITH HIGH TEMPERATURE PEM FUEL CELL SYSTEM) อ.ที่ปรึกษาวิทยานิพนธ์หลัก: ผศ. ดร.อมรชัย อาภรณ์วิชานพ, 91 หน้า.

ในงานวิจัยนี้กระบวนการรีฟอร์มมิงแก๊สชีวภาพแบบเคมิคอลลูปปิงที่มีการดูดซับร่วมกับเซลล์เชื้อเพลิงชนิดเยื่อแลกเปลี่ยนโปรตอนอุณหภูมิสูงถูกนำมาวิเคราะห์ โดยแนวคิดทางเทอร์โมไดนามิกส์และแบบจำลองทางไฟฟ้าเคมีได้ถูกนำมาใช้ในการหาสภาวะที่เหมาะสมในการดำเนินการของกระบวนการที่ได้นำเสนอ การวิเคราะห์ทางเอ็กเซอร์จีและพลังงานถูกใช้ในการอธิบายผลกระทบจากตัวแปรต่างๆเช่น อุณหภูมิในการรีฟอร์มมิง สัดส่วนเชิงโมลของไอน้ำต่อแก๊สชีวภาพ สัดส่วนเชิงโมลของแคลเซียมออกไซด์ต่อแก๊สชีวภาพ และสัดส่วนเชิงโมลของนิกเกิลออกไซด์ต่อแก๊สชีวภาพ ต่อสมรรถนะของระบบ โดยค่าเอ็กเซอร์จีที่สูญเสียในแต่ละหน่วยปฏิบัติการสามารถถูกใช้ระบุคุณภาพทางพลังงานที่ใช้ในแต่ละหน่วยปฏิบัติการ ข้อมูลที่ได้สามารถถูกใช้ในการปรับปรุงทั้งประสิทธิภาพทางพลังงานและเอ็กเซอร์จีของระบบ ผลการจำลองพบว่าประสิทธิภาพทางเอ็กเซอร์จีสามารถถูกปรับปรุงจาก 16.60% สูงขึ้นเป็น 26.72% เมื่อมีการประยุกต์การใช้พลังงานความร้อนร่วมกัน

ภาควิชา วิศวกรรมเคมี ลายมือชื่อนิสิต .....

สาขาวิชา วิศวกรรมเคมี ลายมือชื่อ อ.ที่ปรึกษาหลัก .....

ปีการศึกษา 2558

5770304321 : MAJOR CHEMICAL ENGINEERING
KEYWORDS: SORPTION ENHANCED CHEMICAL-LOOPING / HIGH TEMPERATURE PROTON EXCHANGE MEMBRANE FUEL CELL (HT-PEMFC) / EXERGY ANALYSIS

SARUNYOU KASEMANAND: PERFORMANCE ASSESSMENT OF A BIOGAS SORPTION ENHANCED CHEMICAL LOOPING REFORMING PROCESS INTEGRATED WITH HIGH TEMPERATURE PEM FUEL CELL SYSTEM. ADVISOR: ASST. PROF. AMORNCHAI ARPORNWICHANOP, D.Eng., 91 pp.

In this research, a biogas sorption enhanced chemical looping reforming (SECLR) process integrated with high temperature proton exchange membrane fuel cell (HT-PEMFC)is analyzed. The thermodynamic concept and electrochemical model are used to identify the suitable operating conditions of the proposed process. Exergy and energy analyses are used to describe the effect of various parameters, such as reforming temperature, steam-to-biogas molar ratio, CaO-to-biogas molar ratio and NiO-to-biogas molar ratio, on the process performance. The exergy destruction of each unit is employed to identify the quality of energy that is used in each unit. The data obtained can be used to improve the energy and exergy efficiencies of the process. The simulation results show that the exergy efficiency of the process is improved from 16.60% to 26.72% when a process heat integration is applied.

Department: Chemical Engineering Student's Signature .....
Field of Study: Chemical Engineering Advisor's Signature .....
Academic Year: 2015

ACKNOWLEDGEMENTS

First of all, I would like to express the deepest appreciation to my thesis advisor, Assistant Professor Dr. Amornchai Arpornwichanop for the continuous support of my research, immense knowledge and useful suggestion throughout this research.

I would also like to thank the member of thesis committee, Associate Professor Dr. Soorathep Kheawhom, Dr. Pimporn Ponpesh and Dr. Suthida Authayanun for their time and valuable comments on this thesis.

Moreover, I would like to thank Dr. Phanicha Tippawan and Mr. Nuttawut Visitdumrongkul, for giving me process simulation knowledge and exergy analysis guidance.

Financial support by Chulalongkorn Academic Advancement into its 2nd Century Project, National Research University Project from Office of Higher Education Commission and Ratchadaphiseksomphot Endowment Fund is gratefully acknowledged.

Furthermore, I am very grateful to the Department of Chemical Engineering, Chulalongkorn University for providing the scholarship during my Master's degree study.

Finally, I am forever grateful my beloved family, especially my parents for all the love and the great encouragement. Thanks to my friends in the Control and Systems Engineering Research Laboratory and Computational Process Engineering Research Unit for all their support throughout this research.

CONTENTS

Page

THAI ABSTRACT iv
ENGLISH ABSTRACT v
ACKNOWLEDGEMENTS vi
CONTENTS vii
LIST OF TABLES xi
NOMENCLATURES xv
CHAPTER I INTRODUCTION 1
1.1 Background and motivation 1
1.2 Research Objectives 6
1.3 Scopes of work 6
1.4 Expected output 7
CHAPTER II LITERATURE REVIEWS 8
2.1 Biogas reforming process 8
2.1.1 Steam reforming of biogas 9
2.1.2 Autothermal reforming of biogas 10
2.1.3 Dry reforming of biogas 10
2.2 Sorption enhanced chemical looping reforming (SECLR) process 11
2.3 High temperature proton exchange membrane fuel cells (HT-PEMFCs) 12
2.4 HT-PEMFCs system integrated with reforming processes 13
2.5 Exergy analysis 14
CHAPTER III THEORY 15
3.1 Chemical looping concept 15
3.1.1 Chemical looping combustion 15
3.1.2 Chemical looping reforming 16
3.1.3 Calcium looping reforming 18
3.1.4 Sorption enhanced chemical looping reforming 18
3.1.5 Reforming process model 20
3.2 Proton exchange membrane fuel cells (PEMFCs) 22

Page

3.2.1 Basic principle of fuel cells 22
3.2.2 Proton exchange membrane fuel cells (PEMFCs) 23
3.2.2.1 Basic principle of PEMFCs 23
3.2.3 Disadvantage in conventional PEMFCs 25
3.2.3.1 Water management problem 25
3.2.3.2 CO poisoning problem 26
3.2.4 High temperature proton exchange membrane (HT-PEMFCs) 26
3.3 Mathematical model of HT-PEMFCs 27
3.3.1 Electrochemical model 27
3.3.1.1 Voltage losses 29
Activation loss 29
Ohmic loss 31
Concentration losses 31
3.4 Exergy Analysis 33
CHAPTER IV Modeling of SECLR process and HT-PEMFC 36
4.1 SECLR simulation 36
4.1.1 Selection of thermodynamic method 37
4.1.2 Specification of components 37
4.1.3 Setup for simulation 40
4.1.4 SECLR flow sheet configuration 40
4.2 HT-PEMFCs simulation 43
4.3 Model Validation 44
CHAPTER V Thermodynamic analysis of a SECLR process for hydrogen production 48
5.1 Analysis of operating parameters 48
5.2 Results and discussion 49
5.2.1 CO_2 capture effect on chemical looping reforming process 49
5.2.2 Effect of steam-to-biogas molar ratio (S/B) and reforming temperature 51

Page

5.2.3 Effect of nickel oxide-to-biogas molar ratio (NiO/B) and reforming temperature on hydrogen purity and yield. 52
5.2.4 Effect of nickel oxide-to-biogas molar ratio (NiO/B) on the concentration of CO in reformate gas 54
5.2.5 Effect of nickel oxide-to-biogas molar ratio (NiO/B) on the net energy demand for the SECLR process 55
5.2.6 Carbon formation in a SECLR process 56
5.2.7 Effect of nickel oxide-to-biogas molar ratio (NiO/B) and calcium oxide-to-biogas molar ratio (CaO/B) on the SECLR process 58
5.3 Conclusion 59
CHAPTER VI Energy analysis of a SECLR process and HT-PEMFC integrated system 60
6.1 Analysis of a SECLR process and HT-PEMFC integrated system 60
6.2 Result and discussion 62
6.2.1 Effect of steam to biogas ratio on the thermal efficiency of SECLR process 62
6.2.2 Effect of utilization factor on the efficiency of HT-PEMFC 65
6.2.3 Effect of utilization factor on the heat recovery from HT-PEMFC 65
6.3 Conclusion 66
CHAPTER VII EXERGY ANALYSIS 67
7.1 Result and discussion 68
7.1.1 Energy integration analysis 69
7.1.2 Effect of steam to biogas ratio on exergy destruction of SECLR process 73
7.1.3 Effect of NiO to biogas ratio on exergy destruction and heat recovery from air reactor of SECLR process 74
7.1.4 Effect of cell temperature on exergy destruction and exergy efficiency 76
7.1.5 Effect of operating current density on exergy destruction and exergy efficiency 78
7.1.6 Process improvement using exergy analysis 79

Page

7.2 Conclusion 83
CHAPTER VIII CONCLUSION AND RECOMMENDATION 85
8.1 Conclusion 85
8.2 Recommendation 86
REFERENCES 87
VITA 91

LIST OF TABLES

Table **Page**

Table 4.1 Reaction involved in SECLR process. 38

Table 4.2 Biogas molar compositions (Gopaul et al., 2015). 39

Table 4.3 Specification components. 39

Table 4.4 Process description 42

Table 4.5 The values of the parameters used for HT-PEMFC modelling. 44

Table 4.6 Comparison of simulation data and experimental data. 46

Table 4.7 Comparison of simulation data and experimental data. 47

Table 5.1 Comparison of hydrogen purity of CLR process and SECLR process . 50

Table 6.1 Thermal efficiency of SECLR process operated with biogas 1 kmol/hr and different S/B ratios at reforming temperature 500 ºC. 63

Table 6.2 Mole fraction and mole flowrate of hydrogen at different steam to biogas ratio 64

Table 7.1 The standard chemical exergy of substances 68

Table 7.2 Suitable operating conditions for hydrogen production from biogas SECLR process 70

Table 7.3 Descriptions of streams 71

Table 7.4 Heat duty and exergy destruction of each unit. 72

Table 7.5 Exergy destruction of each unit using in HT-PEMFC simulation 77

Table 7.6 Exergy analysis of each unit process 81

Table 7.7 Comparison of exergy efficiency and thermal efficiency of this system 83

LIST OF FIGURES

Figure **Page**

Figure 3.1 Scheme of a chemical looping combustion system. (Adanez et al., 2012) 15

Figure 3.2 Schematic representation of chemical looping combustion process. .. 16

Figure 3.3 Schematic representation of chemical looping reforming process. 17

Figure 3.4 Schematic of the calcium looping process (Dieter et al., 2014) 18

Figure 3.5 Types of fuel cells, their operating temperatures and reactions (Barbir, 2012) 22

Figure 3.6 A single PEM fuel cell configuration (Spiegel, 2008) 24

Figure 3.7 The basic principle of operation of a PEM fuel cell. (BARBIR, 2012) 25

Figure 3.8 Typical polarization curve of PEMFCs (Jiang et al., 2011) 28

Figure 3.9 Exergy balance on the system 33

Figure 4.1 Flowsheet of SECLR simulation. 40

Figure 4.2 Flowsheet of HT-PEMFC simulation 43

Figure 4.3 Comparison of model prediction and experimental data of Rydén and Ramos (2012) 45

Figure 4.4 Comparison of model prediction and experimental data of Rydén and Ramos (2012) 46

Figure 4.5 Comparison between modelled and experimental polarization curve. 47

Figure 5.1 Schemetic description of SECLR process 49

Figure 5.2 Effect of S/B ratio on mole fraction of hydrogen with dry basis at NiO/B ratio of 0.5, CaO/B ratio of 1 and different temperature. 51

Figure 5.3 Effect of S/B ratio on hydrogen yield at NiO/B ratio of 0.5, CaO/B ratio of 1 and different temperature. 52

Figure 5.4 Effect of NiO/B ratio on mole fraction of hydrogen with dry basis at S/B ratio of 2, CaO/B ratio of 1 and different temperature. 53

Figure 5.5 Effect of NiO/B ratio on hydrogen yield at S/B ratio of 2, CaO/B ratio of 1 and different temperature..... 54

Figure 5.6 Effect of NiO/B ratio on mole fraction of carbonmonoxide with dry basis at S/B ratio of 2, CaO/B ratio of 1 and different temperature..... 55

Figure 5.7 Effect of NiO/B ratio on the net energy of SECLR process at S/B ratio of 2, CaO/B ratio of 1 and different temperature..... 55

Figure 5.8 Effect of CaO/B ratio and S/B ratio on the amount of carbon formation at NiO/B ratio of 0.5 and 500 ºC..... 57

Figure 5.9 Effect of S/B ratio and reforming temperature on the amount of carbon formation at NiO/B ratio of 0.5 and CaO/B of 1. 58

Figure 5.10 Effect of NiO/B ratio and CaO/B ratio on mole fraction of hydrogen at S/B ratio of 2 and 500 ºC. 59

Figure 6.1 Polarization curve and power density of the HT-PEMFC..... 64

Figure 6.2 Effect of operating current density on fuel cell efficiency with different fuel utilization factor..... 65

Figure 6.3 Effect of U_f on heat recovery from HT-PEMFC at S/B ratio of 2 and cell temperature 160 ºC..... 66

Figure 7.1 A schematic of SECLR process before exergy efficiency improvement 69

Figure 7.2 A comparison of exergy destruction of SECLR process operated with S/B ratios of 1 and 2..... 73

Figure 7.3 Exergy destruction of each unit with different NiO/B ratio 74

Figure 7.4 Heat recovery of SECLR process at various NiO/B ratios..... 75

Figure 7.5 The exergy efficiency of SECLR process at various NiO/B ratio..... 76

Figure 7.6 A schematic of a HT-PEMFC using in this system..... 76

Figure 7.7 Exergy destruction of fuel cell at different cell temperature 77

Figure 7.8 Effect of operating current density on exergy efficiency with different temperature. 78

Figure 7.9 Effect of S/B ratio on exergy efficiency with different cell temperature 79

Figure 7.10 A schematic of SECLR and HT-PEMFC integrated system..... 80

Figure 7.11 Percentage of exergy destruction of each unit. 82

NOMENCLATURES

a_c	Catalyst surface area (cm^2/g)
a_{H_2O}	Water activity in the thin film
b	Tafel slope
C_{O_2}	Concentration of oxygen at the channel inlet (mol/cm^3)
C_{Pt}	Concentration at the catalyst surface (mol/cm^3)
C_{ref}	Reference concentration (mol/cm^3)
$D_{O_2}^{eff}$	Effective oxygen diffusivity (cm^2/s)
E_c	Activation energy (J/mole/K)
E_{cell}	Cell voltage (V)
Ex_Q	Exergy of thermal energy (W)
Ex_W	Exergy of work (W)
ex_{ph}	Specific physical exergy (J/mole)
ex_{ch}	Specific chemical exergy (J/mole)
f_i	Fugacity of species i
F	Faraday's constant (C/mol)
G^t	Total Gibbs free energy
ΔH^o_{298K}	Enthalpy of formation
ΔH_T	Enthalpy of water formation (J/mole)
i	Current density (A/m^2)

NOMENCLATURES

i_0	Exchange current density (A/m^2)
i_0^{ref}	Current density at a reference temperature (A/m^2)
i_L	Limiting current density (A/m^2)
κ_m	Ion conductivity (Km)
LHV_i	Low heating value of specie i
L_c	Catalyst loading
l_m	Transfer coefficient (cm)
l_d	Thickness of GDL (cm)
n_i	Amount of each gaseous component
$P_{H_2O}^{sat*}$	Saturated water vapour pressures (atm)
P_{FC}	Electrical power output of fuel cell (W)
R	Gas constant (8.314 J/mol /K)
ΔS_T	Entropy of water formation (J/mole/K)
T	Cell temperature (K)

Greek symbol

α	Transfer coefficient
η_a	Anode activation overpotential
η_c	Cathode activation overpotential (V)

NOMENCLATURES

η_{conc}	Concentration overpotential (V)
η_{ohmic}	Ohmic overpotential (V)
α	Transfer coefficient
σ_d	Electrical conductivity of the gas diffusion electrode (S/cm)
γ	Reaction order
μ_i	Chemical potential of species i

CHAPTER I
INTRODUCTION

1.1 Background and motivation

At present, the world energy-resources are primarily obtained from the fossil fuels, which are non-renewable and limited resources (Barbir, 2012). In addition, the combustion of fossil fuels to generate heat and electricity is the largest source of greenhouse gas emissions to the atmosphere that leads to global warming. For these reasons, the research and development of clean alternative energy become important.

Fuel cells are considered for clean power generation because they have high efficiency and produce low environmental pollution (Shamardina et al., 2010). As the fuel cell is a source of electricity generation without involving any moving parts, they can operate silently. Fuel cells are usually powered by pure hydrogen or hydrogen rich gas which can be obtained by a reforming process. A reformer converts hydrocarbon to a hydrogen rich gas by chemical reactions (Gou et al., 2009). Typically, most hydrogen rich gas can be produced by reforming of natural gas which its availability is limited (NREL, 2014). The key to solve such a problem is to find new sustainable resources for hydrogen production.

Biogas is an attractive renewable fuel source which can be produced when bacteria decomposes the organic matters such as wastewater, agricultural wastes, animal manure and green waste. Biogas mainly consists of 50-85% CH_4, 20-35% CO_2, H_2, N_2, and H_2S. Typically, the composition of biogas depends on the type of substrate and the design process (Herout et al., 2011). The use of biogas can reduces the emission

of primary greenhouse gases, CH_4 and CO_2, into the atmosphere (A. Lima da Silva et al., 2012). In addition, the main advantage includes a sustainable waste management (Seadi et al., 2008). To produce hydrogen from biogas, the reforming technology for natural gas, such as steam reforming, partial oxidation and auto-thermal reforming, can be applied for biogas. However, in the biogas reforming, a pretreatment unit, such as a desulphurization unit to purify feed which can prevents the catalyst deactivation is required. In general, the steam reforming can give the highest hydrogen production, but it needs high energy inputs. In the partial oxidation, sub-stoichiometric fuel is mixed with enough oxygen to be converted to hydrogen and carbon monoxide. Partial oxidation is exothermic reaction and thus, the heat requirements are negligible. However, the partial oxidation process provides the lowest hydrogen yield and the amount of oxygen is carefully controlled for preventing complete reaction (Wang and Rohr, 2002). The autothermal reforming is a combination of steam reforming with partial oxidation which can balance the heat requirements.

Recently, the chemical looping reforming (CLR) technology is proposed to overcome the drawbacks of conventional reforming. The CLR process involves both steam reforming and partial oxidation. The advantage of CLR is the use of metal oxide instead of pure oxygen and thus, the operating cost is lower than ATR. A CLR system consists of two fluidized-bed reactors: fuel reactor (FR) and air reactor (AR). Fuel for hydrogen production is fed to FR in which fuel is oxidized using metal oxide as a solid oxygen carrier. For the CLR, nickel oxide is known to be a suitable oxygen carrier (Rydén et al., 2006). The reaction in the FR should be partial oxidation by using low nickel oxide to fuel molar ratio. The AR or solid oxidation reactor (SR) in where nickel obtained from the oxidation of fuel with nickel oxide is converted to nickel oxide which

is recycled to the FR. To enhance the performance of CLR process, a sorption enhanced chemical loop reforming (SECLR) has been proposed by Rydén and Ramos (2012). The addition of CO_2 sorbents in the SECLR results in the production of hydrogen with high purity; the removal of CO_2 during the course of the reforming reaction can shift the reaction forward to a hydrogen product side (Nalbandian et al., 2011).

A proton exchange membrane fuel cell (PEMFC) is among the various types of fuel cells that are received considerable attention due to high efficiency, high power density and zero-emission. In general, PEMFC can be operated with pure H_2 or H_2-riched gas as a fuel and O_2 from the air as an oxidant. It consists of a negatively charged electrode (anode), a positively charged electrode (cathode) and an electrolyte membrane. The membrane material for PEMFC is usually made of perfluorocarbon-sulfonic (Nafion^{TM}). PEMFC presently operates at temperatures below the boiling point of water as the Nafion^{TM} membrane typically used in low temperature fuel cells requires a good water management for effective proton conductivity (Cheddie and Munroe, 2006). The advantages of low temperature proton exchange membrane fuel cells (LT-PEMFCs) are rapid start up and long endurance (Welaya et al., 2012). However, the platinum catalyst in the anode is quickly deactivated by CO poisoning. In addition, the Nafion^{TM} membrane is extremely required water management to prevent dehydration at low current densities and excessive water at high current densities. These problems can be solved by operating the PEMFC at higher temperatures which is known as a high temperature proton exchange membrane fuel cells (HT-PEMFCs).

The HT-PEMFC typically operate at temperatures from 90 to 200°C and low humidity (Zhang et al., 2013). Thus, the water management can be neglected. Polybenzimidazole-based phosphoric acid-doped acid are usually used as membrane for HT-PEMFC. The performance of HT-PEMFC is improved and stand for contaminants in a hydrogen rich gas because an increase in the operating temperatures favors H_2 adsorption over CO adsorption on Pt catalyst. In addition, the electrode's kinetics is increased.

At present, there are various technologies to produce electricity from biogas on a household level. The amount of organic waste which can used to produce biogas is enough to use as fuel for electricity in industry-scale application. Pariphat and Supawat 2012 presented that the amount of 94.19 ton/day waste from Talad-Thai market in Thailand can be converted to biogas 17,807 m^3/day and then they can used to produce electricity at 0.53-1.04 MW. Typically, biogas is mostly used as fuel for combustion engines, which are operated by the burning of fuel to produce electricity. In previous studies, they obtained electrical power efficiency around 22-29% from internal combustion electrical generator units from biogas which consisted of 55% methane (Brain, 2009). In addition, Yingjian et al. 2014 present the exergy efficiency and energy efficiency of internal combustion engine using biogas are 27.36% and 28.45%, respectively. However, the previous studies which used biogas as fuel for electricity generator are low efficiency. Therefore, the new technologies must be considered. In this study, the suitable process which can produce electricity from biogas is purposed by reforming process and HT-PEMFC integrated system. However, the main problem of using biogas to produce H_2 rich gas for HT-PEMFC is the CO_2 contamination that can be converted to CO in reforming process and then it can be anode catalyst

poisoning. Therefore, the new reforming concept which is enhanced by CO_2 capture and fuel cell integrated process are purposed to produce electricity from biogas. The performance of HT-PEMFC system integrated with a SECLR process is investigated by to generate electricity from biogas fuel. The simulation model of such an integrated process is developed by using Aspen Plus program. The developed process model will be used to find suitable operating conditions of the SECLR process to produce hydrogen for the HT-PEMFC. Then, the data which are obtained from the simulation are used to analyze in term of system efficiency. The energy and exergy analysis are used as tools to identify the defects of process. They can used to improve efficiency of process. Energy and exergy analysis of the SECLR and HT-PEMFC integrated system are performed for understanding of fuel conversion mechanism and energy utilization in the system. Then, this study investigates how to achieve the higher efficiency energy and exergy of the process.

1.2 Research Objectives

1. To simulate the sorption enhanced chemical looping reforming (SECLR) process integrated with high temperature proton exchange membrane fuel cells (HT-PEMFCs) running on biogas.

2. To investigate the effects of operating parameters on the performance of SECLR process integrated with HT-PEMFCs.

3. To investigate the thermodynamic performance from energy and exergy of SECLR process integrated with HT-PEMFCs.

1.3 Scopes of work

1. Modeling of the SECLR process integrated with HT-PEMFCs with Aspen Plus software.

2. To investigate the suitable operating conditions of the SECLR integrated with HT-PEMFCs system such as, reforming temperatures, steam to biogas ratios (S/B), NiO to biogas ratios (NiO/B), CaO to biogas ratios (CaO/B) and to find the energy efficient system configuration.

3. Analysis of the energy and exergy efficiency of SECLR process running with biogas.

4. Improve the energy and exergy efficiency of the SECLR integrated with HT-PEMFCs system running with biogas by heat integration.

1.4 Expected output

A new approach to obtain the high performance integrated system and suitable operating conditions that can generate electricity from biogas with low-emissions by using SECLR process and HT-PEMFC integrated system and then this process obtains the achievement higher energy and exergy efficiency than conventional processes.

CHAPTER II
LITERATURE REVIEWS

Several studies on PEMFCs integrated with reforming process have been reported in the recent literature. This chapter will present the literature reviews of sorption enhance chemical looping reforming (SECLR) and high temperature proton exchange membrane fuel cells (HT-PEMFCs). The literature reviews divide into four parts. First, biogas reforming from various process is reviewed in section 2.1. Second, the reviews of SECLR process are described in section 2.2. Third, analysis of HT-PEMFCs are described in detail of performance in section 2.3. Finally, the PEMFCs system integrated with reforming processes are revealed in section 2.4.

2.1 Biogas reforming process

The crisis in energy and global warming have been instigating the research for new technologies and renewable energy sources. Consequently, the interest in hydrogen as a sustainable energy carrier has been increasing due to high heating value, clean energy and low emission. Hydrogen is derived from non-renewable resources such as fossil fuels and primarily natural gas. However, hydrogen can be generated from renewable resources such as biogas by steam reforming process. Biogas is considered for renewable resource that prevents the emission of methane. Commonly, the composition of biogas is mainly based on methane and carbon dioxide. Biogas can be an alternative raw material to conventional reforming process (Braga et al., 2013). Chattanathan et al. (2014) investigated the effect of major impurity (i.e., H_2S) on a commercial methane reforming catalyst. The research found that small amount of H_2S

(0.5 mol%), the conversion of CH_4 and CO_2 was dropped about 20%. For fuel cells, the development of alternative technologies to produce high purity hydrogen should be studied.

2.1.1 Steam reforming of biogas

The steam reforming is mostly used in the hydrogen production process. Typically, biogas consists of 50-85% CH_4, 20-35% CO_2, 1% H_2O, 100-800 ppm NH_3 and 1000-3000 ppm H_2S. For high purity hydrogen production from biogas steam reforming, such formed products as CO and CO_2 besides other by-products should be separated. The steam reforming system requires a desulphurization unit as pretreatment process due to the deactivation of Ni catalyst. In addition, the commercial Ni-based catalysts and subsequent reactor are also deactivated by the use of biogas with CH_4/CO_2 ratio >1. Effendi et al. (2005) studied the steam reforming of clean model biogas in a fluidized-bed reactor followed by two stages of CO shift reactors. The results are an almost complete CH_4 more than 98% conversion and strong inhibition of carbon formation can be obtained by excess steam. The optimization of H_2 production and CO shift reactions by using commercial catalysts, based on Cu/Fe/Cr and Cu/Zn, respectively were at high temperatures (523-723 K) and low temperatures (423-523 K). For the biogas steam reforming over 5% Ru/Al_2O_3 catalyst, Avraam et al. (2010) developed a theoretical model of the process, the main reactions were steam reforming and water gas shift. The results and theoretical predictions of the catalyst stability was assured and optimal operation was identified at temperature from 973 to 1,073 K, CH_4/CO_2 ratio ranging from 1.0 to 1.5 and H_2O/CH_4 ratio ranging from 3.0 to 5.0. The effect of CO_2/CH_4 ratio on the biogas steam reforming was investigated by Zhu et al.

(2014). The increasing of CO_2/CH_4 ratio effected CH_4 and CO_2 conversion increased. The highest conversion of CO_2 appeared at CO_2/CH_4 ratio of 0.67.

2.1.2 Autothermal reforming of biogas

The autothermal reforming (ATR) of biogas over Ni based monolithic catalyst was studied by Araki et al. (2010). The suitable start-up conditions, the steam should be supplied at temperature higher than 723 K due to the deactivation of Ni based catalyst at steam feed temperatures below 723 K. The CH_4 conversions at all examined temperatures were higher than the equilibrium conversion calculated due to the heat from exothermic catalytic partial oxidation reaction on catalyst layer. Furthermore, the O_2/C ratios > 0.42, the CH_4 conversion was higher than the equilibrium conversion and reached about 100% at O_2/C equal to 0.55. In a term of hydrogen production, the O_2/C ratios of 0.45-0.55 and S/C ratios of 1.5-2.5 could obtain the highest hydrogen concentrations and CH_4 conversions.

2.1.3 Dry reforming of biogas

Gopaul et al. (2015) studied the dry reforming of methane (DRM) from biogas in terms of H_2 and CO yield. This study was divided in three cases, case 1 DRM alone, case 2 DRM and partial oxidation (POX), case 3 DRM and hydrogen oxidation (HOX). Three cases were investigated by Aspen Plus simulation software which the method of Gibbs free energy minimization at specific components of inlet flowrates, operating temperature and pressure was used for investigation. In case 1 DRM alone, the results show that increasing operating temperature also affected molar flowrates of H_2 and CO increased and the optimal operating temperature and pressure were 950 ºC and 1 atm. However, DRM alone demanded high energy supply due to extremely endothermic

process. Thus, case 2 and case 3 were considered for thermo-neutrality. Case 2, syngas at thermo-neutrality was smaller amounts of H_2 and CO_2 than case 1 because the CO_2 and H_2O combustion product dilute the H_2 purity. Case 3, the combined DRM-HOX process, excess H_2 was required for thermo-neutrality, the result shows that the effect of dilution was not occurred by combustion product.

2.2 Sorption enhanced chemical looping reforming (SECLR) process

The use of renewable energy resources is possible to approach minimize greenhouse gas emissions. Furthermore, a way to reduce CO_2 emissions, that is the CO_2 capture in an emission source. The several methods of CO_2 capturing have been studied for reducing CO_2 emissions. Chemical looping combustion (CLC) can be used for CO_2 capture in power generating, which should avoid the direct contact between fuel and combustion air. A solid oxygen carrier is used to bringing oxygen to the fuel. Metal oxides e.g. NiO, Fe_2O_3, Mn_3O_4, CuO, CoO, Co_3O_4, Mn_2O_3 and NiO are suitable solid oxygen carriers. In CLC process, the oxygen carrier is reduced in the fuel reactor by the oxidizing fuel. Then, the oxygen carrier is oxidized in the air reactor by air. The CLC process has been focused on minimizing CO_2 emissions. For hydrogen production, chemical looping reforming (CLR) is a method for partial oxidation of fuel which use the solid oxygen carrier as a source of undiluted oxygen.

In terms of high purity hydrogen production by SECLR, Dou et al. (2014) experimentally studied the continuous high-purity hydrogen production by SECLR of glycerol base on redox reactions integrated with in situ CO_2. The experiment used two moving bed reactors for a flow of catalyst and sorbent mixture. The low-cost $NiO/NiAl_2O_4$ was used as catalyst and the CaO sorbent used for the CO_2 removing. The results achieved that the reduced Ni could be oxidized to NiO by air at 1173 K. In

addition, the catalyst and sorbent could be regenerated under the same conditions in air reactor. Pimenidou et al. (2010) studied SECLR of waste cooking oil (WCO) in a packed bed reactor was analyzed under autothermal operation. The study illustrated the ability of the CO_2 sorbent to repeatedly carbonate over 6 cycles at 873 K, the WCO and steam conversions were 0.9 and 0.27 respectively on 80 g of the NiO-Al_2O_3 catalyst. On the other hand, when the catalyst used only 40 g of catalyst compared with 40 g of catalyst calcined + 40 g dolomite, the results show that the WCO and steam conversions on 40 g of catalyst calcined + 40 g dolomite were larger than the catalyst without the sorbent.

2.3 High temperature proton exchange membrane fuel cells (HT-PEMFCs)

The increasing interest in clean energy generator technologies generates a huge amount of research on fuel cell systems due to higher efficiency and zero emission. Proton exchange membrane fuel cells (PEMFCs) are considered an alternative for distributed source of energy. PEMFCs or low temperature PEMFCs (LT-PEMFCs) usually operate at temperature < 90 ºC. However, PEMFCs have several problems during operation such as low tolerance for contaminants, complicated water management and heat management. In case of reformate gas supply, the reformate gas from the reformer is directly used as fuel for PEMFCs thus, the impurities in a reformate gas can be catalyst poisoning. To solve some of the problems of LT-PEMFCs, Scott et al. (2007) found that PEMFCs performance operated on reformate gas can be improved high operating temperature. Recently, the developed HT-PEMFCs based on acid-doped PBI membranes can tolerate a few percent of CO in the reformate gas at the same temperature range. The advantages of acid-doped PBI are acceptable conductivity up to 200 ºC, good mechanical strength and chemical stability at high temperature. In

addition, the humidification was not necessary because a H_3PO_4-doped polybenzimidazole (PBI) membrane of HT-PEMFCs can be operated at a temperature as high as 200 ºC without water management.

2.4 HT-PEMFCs system integrated with reforming processes

Araya et al. (2012) studied the effects of reformate gas impurities on a H_3PO_4-doped polybenzimidazole (PBI) membrane of HT-PEMFCs. The results confirmed that CO is the most degrading agent of all the impurities and CO_2 has only minor effects. At CO concentration of 2% by volume, the result showed that tolerance to CO of a PBI-based HT-PEMFCs was reduced in the presence of CO_2. Herdem et al., (2015) investigated that the CO in the reformate gas increased with a low steam/carbon ratio and high temperature operation. The effect of CO on the fuel cell performance decreased at high temperature that fuel cell temperature at 160 ºC and 0.9% CO molar decreased around 78% of fuel cell voltage. When fuel cell temperature increased from 160 ºC to 180 ºC, fuel cell voltage decreased around 61%. O. Shamardina et al. (2010) developed a simple model of a HT-PEMFCs which model was pseudo two dimensional, steady-state and isothermal. The empirical correlations can be used to calculate the effective oxygen diffusivity for a given temperature, pressure and gas diffusion layer (GDL) porosity ε. In a term of hydrogen crossover, the permeation coefficient of hydrogen was assumed to be four times greater than the oxygen permeation coefficient from the experiment. The cathode activation and membrane thickness was the highest of voltage loss. Although, the thinner membrane had lower resistant, the crossover effect was higher. The voltage loss could be increased at high current density due to the lack of oxygen by crossover effect.

2.5 Exergy analysis

Exergy analysis is a thermodynamic analysis technique base on the second law of thermodynamics which can identify the causes, locations and magnitudes of process inefficiencies. The advantages of exergy analysis compared to energy analysis are numerous such as exergy losses can identify the locations, causes and sources of deviations from ideality in a system and energy analysis generally fails to identify waste or the effective use of fuels and resources (Dincer and Rosen, 2012).

Hajjaji et al. (2014) investigated the exergetic efficiency of hydrogen production by glycerol autothermal reforming (ATR). The results showed that the exerthermic efficiency of this process was 57% and that 152 kJ was consumed to generated 1 mol of hydrogen. Dimopoulos et al. (2013) presented the exergetic analysis and optimization of a steam methane pre-reforming (SMR) system. They found the SMR system exergy losses amount to 10% in the initial and 5% in the optimal design of the chemical exergy of the overall system's fuel. Wang et al. (2013) studied energy and exergy analysis of a new hydrogen-fueled power plant based on calcium looping process. The result showed that energy and exergy efficiencies of system were 42.7% and 42.25% respectively.

CHAPTER III

THEORY

3.1 Chemical looping concept

A new concept in a term of chemical looping for fuels conversion, which is based on cyclic reduction and oxidation of a solid oxygen carrier to avoid direct contact between fuel and oxygen.

3.1.1 Chemical looping combustion

The majority of the chemical looping combustion (CLC) plants typically use the configuration composed of two interconnected fluidized-bed reactors that consist of a fuel reactor and an air reactor. First, the fuel is oxidized to CO_2 and H_2O in a fuel reactor by a metal oxide that is reduced to metal. Second, the reduced oxygen carrier is oxidized with air to metal oxide, then metal oxide regenerates to start a new cycle. Typically, Fe_2O_3, Mn_3O_4, CuO and NiO are suitable oxygen carriers for CLC process.

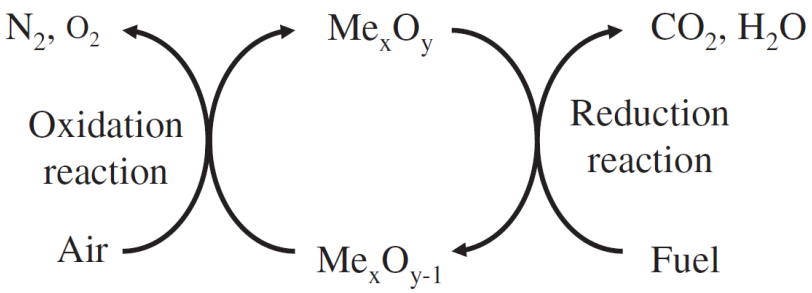

Figure 3.1 Scheme of a chemical looping combustion system. (Adanez et al., 2012)

Reduction $(2n+m)MeO_x + C_nH_{2m} \rightarrow (2n+m)MeO_{x-1} + mH_2O + nCO_2$ (R1)

Oxidation $MeO_{x-1} + \frac{1}{2}O_2 \rightarrow MeO_x$ (R2)

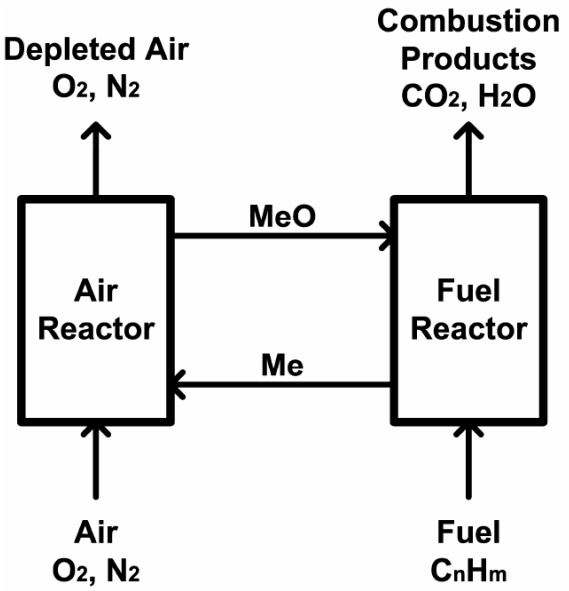

Figure 3.2 Schematic representation of chemical looping combustion process.

3.1.2 Chemical looping reforming

Chemical looping reforming (CLR) uses the same basic principles as CLC but air to fuel ratio must be controlled to prevent complete oxidation. In a term of CLR process, the fuels are partially oxidized using metal oxide to produce a mix of H_2 and CO, instead of being oxidized into CO_2 and H_2O. The advantage of CLR compared to conventional reforming is the energy consumption and cost to air separation is eliminated due to oxygen carrier is used as an oxygen source. Furthermore, the effect of N_2 dilution on products can be neglected. Fuel gas is converted to synthesis gas in the fuel reactor (FR) by partial oxidation.

Partial oxidation $C_nH_m + nMeO_x \rightarrow nCO + \frac{1}{2}mH_2 + mMeO_{x-1}$ (R3)

Complete oxidation

$$C_nH_m + \left(2n + \frac{1}{2}m\right)MeO_x \rightarrow nCO_2 + \frac{1}{2}mH_2O + \left(2n + \frac{1}{2}m\right)MeO_{x-1} \quad \text{(R4)}$$

Steam reforming $C_nH_m + nH_2O \rightarrow \left(n + \frac{1}{2}m\right)H_2 + nCO$ (R5)

CO_2 reforming $C_nH_m + nCO_2 \rightarrow \frac{1}{2}mH_2 + 2nCO$ (R6)

Water-gas shift $CO + H_2O \rightarrow CO_2 + H_2$ (R7)

Regeneration $MeO_{x-1} + \frac{1}{2}O_2 \rightarrow MeO_x$ (R8)

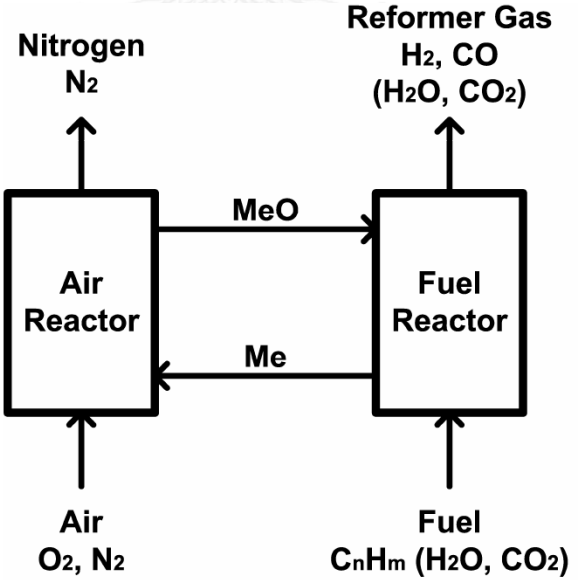

Figure 3.3 Schematic representation of chemical looping reforming process.

3.1.3 Calcium looping reforming

From previous studies, the CaO is interested in CO_2 adsorbent due to there are high CO_2 adsorption capacity, selectivity to the CO_2 and good cyclic stability. CO_2 is captured by exothermic carbonation which taking place in the carbonator at 600-700°C. The reaction express below

Carbonation $CaO+CO_2 \rightarrow CaCO_3$ (R9)

For sorbent regeneration, the $CaCO_3$ is calcined by combustion. In the calciner, an endothermic calcination reaction mostly occurring at 850-950°C. Regeneration occurs that show in the following reaction

Calcination $CaCO_3 \rightarrow CaO+CO_2$ (R10)

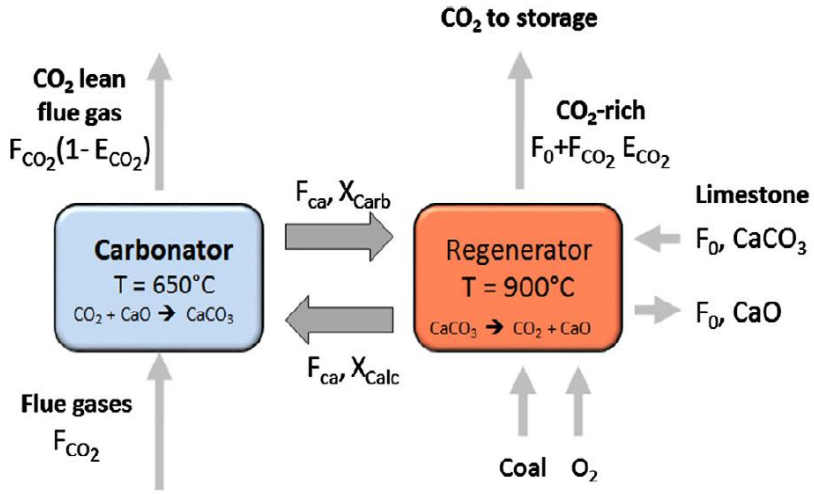

Figure 3.4 Schematic of the calcium looping process (Dieter et al., 2014)

3.1.4 Sorption enhanced chemical looping reforming

To improve steam reforming process, sorption enhanced steam reforming (SESR) which is carried out by adding CO_2 adsorbent into reforming reactor. The benefit of the removal of CO_2 is equilibrium is shifted forward, then more fuel

conversion are achieved. The process of sorption enhanced chemical looping reforming (SECLR) is the combined between sorption enhanced steam reforming (SESR) and chemical looping reforming (CLR) process. In SECLR process, metal oxide and CO_2 adsorbent are employed. The CO_2 formation in processes are captured by CO_2 adsorbent. Thus, this process leads to higher hydrogen purity and more fuel conversion. The main reactions occur in the fuel reactor during the oxygen carrier reduction are

Oxidation

$$CH_4 + 4NiO \rightarrow 4Ni + CO_2 + 2H_2O \qquad \Delta H^{o}_{298K} = 156 \text{ kJ/mol} \qquad \text{(R11)}$$

$$H_2 + NiO \rightarrow Ni + H_2O \qquad \Delta H^{o}_{298K} = -2.1 \text{ kJ/mol} \qquad \text{(R12)}$$

$$CO + NiO \rightarrow Ni + CO_2 \qquad \Delta H^{o}_{298K} = -43.3 \text{ kJ/mol} \qquad \text{(R13)}$$

$$C + NiO \rightarrow Ni + CO \qquad \Delta H^{o}_{298K} = 129.2 \text{ kJ/mol} \qquad \text{(R14)}$$

Partial oxidation

$$CH_4 + NiO \rightarrow Ni + CO + 2H_2 \qquad \Delta H^{o}_{298K} = 169.9 \text{ kJ/mol} \qquad \text{(R15)}$$

Steam reforming catalyzed by Ni

$$CH_4 + H_2O \rightarrow CO + 3H_2 \qquad \Delta H^{o}_{298K} = 205.8 \text{ kJ/mol} \qquad \text{(R16)}$$

Dry reforming

$$CH_4 + CO_2 \rightarrow 2CO + 2H_2 \qquad \Delta H^{o}_{298K} = 247 \text{ kJ/mol} \qquad \text{(R17)}$$

Methane decomposition catalyzed by Ni

$$CH_4 \rightarrow C + 2H_2 \qquad \Delta H^{o}_{298K} = 74.5 \text{ kJ/mol} \qquad \text{(R18)}$$

Carbon gasification

$$C + H_2O \rightarrow CO + H_2 \qquad \Delta H^{o}_{298K} = 131.3 \text{ kJ/mol} \qquad \text{(R19)}$$

$$2CO \rightarrow C + CO_2 \qquad \Delta H^{o}_{298K} = -172 \text{ kJ/mol} \qquad \text{(R20)}$$

Combustion

$$CH_4 + 2O_2 \rightarrow CO_2 + 2H_2O \qquad \Delta H^{o}_{298K} = -806 \text{ kJ/mol} \qquad (R21)$$

Water gas shift

$$CO + H_2O \rightarrow CO_2 + H_2 \qquad \Delta H^{o}_{298K} = -41.2 \text{ kJ/mol} \qquad (R22)$$

In a part of air reactor, the oxygen carrier oxidation

$$Ni + 0.5O_2 + 1.881N_2 \rightarrow NiO + 1.881N_2 \qquad \Delta H^{o}_{298K} = -239 \text{ kJ/mol} \qquad (R23)$$

Global CLR reaction of biogas

$$NiO + CH_4 + CO_2 + H_2O \rightarrow Ni + (C, CO, CO_2, H_2O) + H_2 \text{ Endothermic} \qquad (R24)$$

3.1.5 Reforming process model

For this process, many simultaneous reactions occurs in the fuel reactor. The equilibrium calculations are obtained from the Gibbs energy method. The total Gibbs free energy (G^t) of the system is minimized at the equilibrium state. The total Gibbs free energy is defined as

$$G^{t} = \sum_{i=1}^{N} n_i \mu_i \qquad (1)$$

Where n_i is the number of moles of species i and μ_i is the chemical potential of species i that can be expressed as

$$\mu_i = \overline{G_i^{o}} + RT \ln\left(\frac{f_i}{f_i^{o}}\right) \qquad (2)$$

Where f_i is the fugacity of species i and the superscript ^{o} denotes a standard thermodynamic quantity. R and T are the gas constant and temperature, respectively. Thus, the total Gibbs free energy can be also written as:

$$G^t = \sum_{i=1}^{N} n_i \overline{G_i^o} + \sum_{i=1}^{N} n_i RT \ln\left(\frac{f_i}{f_i^o}\right) \quad (3)$$

The objective function to be minimized is the total Gibbs energy G^t. The problem is to find the values of n_i which is an amount of each gaseous component. Therefore, the equilibrium composition can be determined by solving the minimization problem as follows:

$$\min_{n_i}\left(G^t\right)_{T,P} = \min_{n_i}\left[\sum_{i=1}^{N} n_i\left(\overline{G_i^o} + RT\ln\frac{f_i}{f_i^o}\right)\right] \quad (4)$$

Where $\overline{G_i^o}$ is the Gibbs energy of pure component i at standard condition and N is total number of components in the reaction system. The constraint of this problem is the elemental balance i.e.

$$\sum_{i=1}^{N} a_{ij} n_i = A_j, \quad j = 1,2,1,...,k \quad (5)$$

Where a_{ij} is the number of atoms of element j in component i, A_j is the total number atoms of element j in the reaction mixture and k is the total number of elements.

3.2 Proton exchange membrane fuel cells (PEMFCs)

3.2.1 Basic principle of fuel cells

The first fuel cell is invented by William Groove in 1839. The primary components of fuel cells are a negatively charged electrode (anode), a positively charged electrode (cathode), and an electrolyte membrane. In a galvanic cell, hydrogen is oxidized on the anode and the cathode is the electrode where oxygen is reduced. Then, protons are transported across the electrolyte membrane to the cathode, while the electrons move through the external circuit. Consequently, a fuel cell can convert chemical energy to electrical energy in single step. In addition, the advantages of fuel cells are quiet operation, quick start up and zero emission. The benefit of fuel cells is that is a unique combination of characteristics in one package. For these reasons, a fuel cell becomes the attractive power source for the future.

The various fuel cell can be grouped by the type of electrolyte, that Fig 3.1 summarizes the basic principles of various fuel cell types.

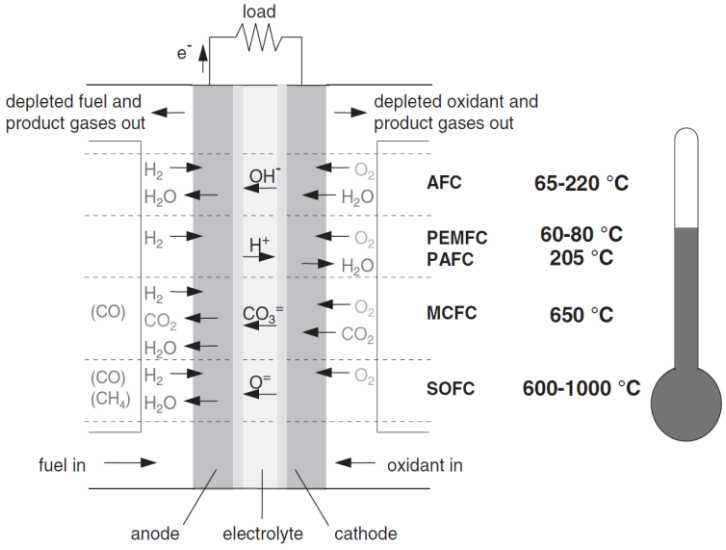

Figure 3.5 Types of fuel cells, their operating temperatures and reactions (Barbir, 2012)

3.2.2 Proton exchange membrane fuel cells (PEMFCs)

Proton exchange membrane fuel cells or polymer electrolyte membrane fuel cells (PEMFCs), are highly efficient electricity generators. PEMFCs use a thin proton conductive polymer membrane as the electrolyte. Typically, Platinum supported on carbon is usually used as the basic catalyst. PEMFCs are the attractive for mobile applications and stationary power generations due to simplicity, noiseless operation, long stack life, quick startup and the operating temperature is low about 60-100 ºC.

3.2.2.1 Basic principle of PEMFCs

PEMFCs consists of two electrodes, in which the cathode and anode are separated by a polymer membrane such as Nafion^{TM}. A core component of PEMFCs is the gas diffusion layer (GDL). The GDL is used to provide conductivity and porous of GDL helps reactant gases in flow channel diffuse into the interface of catalyst layer. Then, the electrochemical reactions that occur on the catalyst layer which is between electrode and electrolyte. The electrodes that cathode and anode are usually made from carbon cloth or carbon fiber paper. Typically, the platinum supported on carbon is used as catalyst. The Nafion^{TM} membrane is typically used as electrolyte, which it can conduct protons from anode to the cathode, while blocking electrons and gases. The electrons move through the outer circuit. Then, the protons and electrons react with oxygen in the feed air. The process produces electricity, water and heat, without gas emissions.

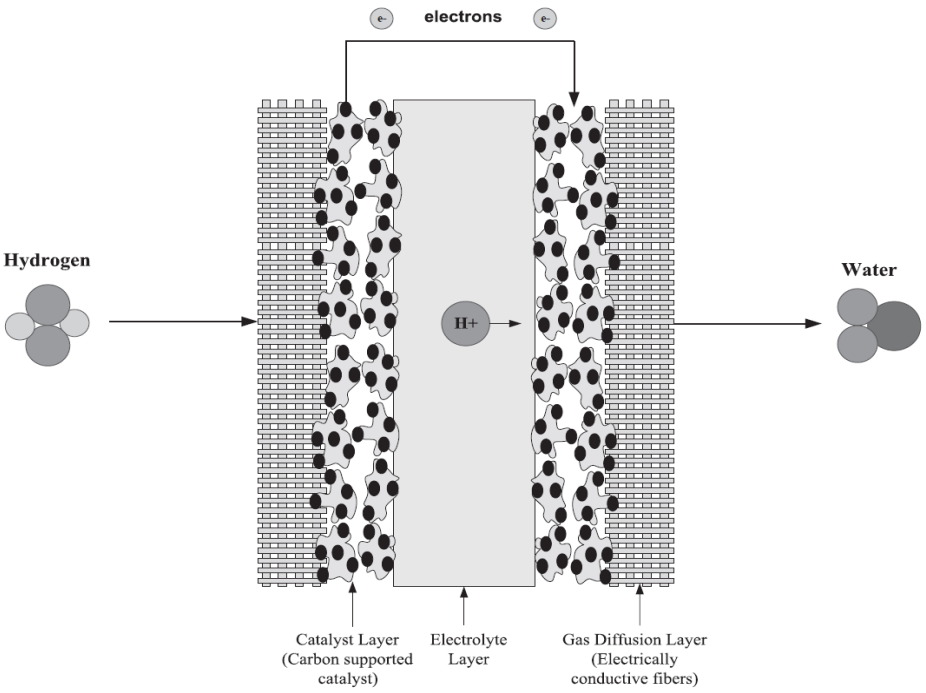

Figure 3.6 A single PEM fuel cell configuration (Spiegel, 2008)

In a term of power generation process, hydrogen rich gas is fed to the anode that is negative electrode, where the oxidation reaction takes place. Then, the reduction reaction of hydrogen occurs as follow:

Anode: $2H_2 \rightarrow 4H^+ + 4e^-$ (R25)

At positive electrode or cathode that oxygen from air in flow channel is fed and combine with protons and electrons.

Cathode: $O_2 + 4H^+ + 4e^- \rightarrow 2H_2O$ (R26)

The electrochemical reaction generates two-phase of water at cathode. Then, the generated water is transported from GDL to the flow channels. Then, the excess flow

of oxygen remove the generated water. Thus, the overall reaction is expressed in Eq. (3.3)

Overall: $2H_2 + O_2 \rightarrow 2H_2O$ (R3)

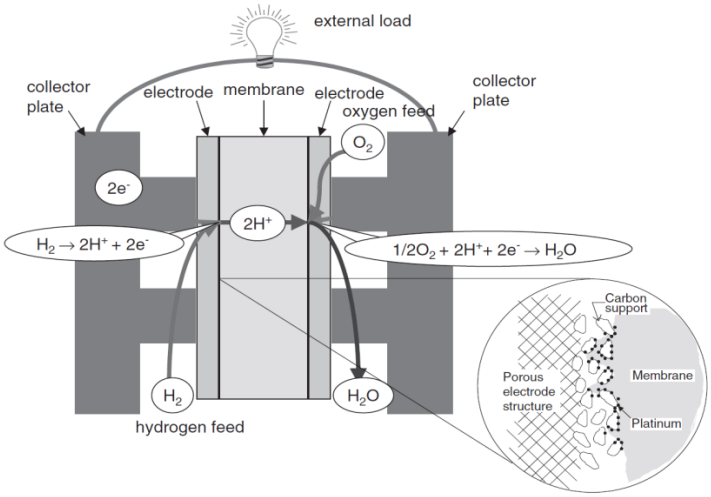

Figure 3.7 The basic principle of operation of a PEM fuel cell. (Barbir, 2012)

3.2.3 Disadvantage in conventional PEMFCs

Conventional PEMFCs typically operate at low temperature. However, there are several hurdles during operation of PEMFCs such as water management problem and CO poisoning problem.

3.2.3.1 *Water management problem*

In PEMFCs, the main of water problem especially occur at the cathode where water is formed in a catalyst layer. Actually, the GDL must permit water to be transported from the electrode/electrolyte interface into the gas flow channels where water is convected out of the fuel cell (Benziger et al., 2005). However, when PEMFCs are operated at high current density, water accumulate at the cathode that hinders

oxygen from getting to the electrode/electrolyte interface causing mass transport limitations. On the other hand, the drying of polymer electrolyte membrane increases the ionic resistance thus, the cell voltage decreases due to the proton conductivity of membrane electrolyte relies on water content.

3.2.3.2 CO poisoning problem

The reformated feed gas usually contain traces of CO. The CO contamination in reformate gases is seriously a poison to platinum electrodes in PEMFCs. The Pt preferentially absorbs the CO, then active catalyst sites are blocked by CO (Amphlett et al., 1996). Thus, the effect of CO increases in activation losses and reduces the voltage output due to catalyst sites available for hydrogen oxidation are limited.

3.2.4 High temperature proton exchange membrane (HT-PEMFCs)

PEMFCs typically operate at lower temperature are high efficiency compared with other devices. However, they have several problems and limitations. For these reasons, there are research advances of high temperature proton exchange membrane fuel cells (HT-PRMFCs) because there are several reasons for operating at high temperature. First, the electrochemical kinetics of electrodes are improved. Second, there would be no liquid water thus, the water management can be simplified. Third, the tolerance to CO is increased allowing the use of the reforming gas. Forth, the cooling system is simplified. Lastly, the waste heat can be used to achieve cogeneration.

3.3 Mathematical model of HT-PEMFCs

The model is used to determine the effect of a range of operating variables and parameters on cell voltage of the PBI-based fuel cell.

3.3.1 Electrochemical model

The overall electrochemical reaction in a PEM fuel cell running on H_2 as fuel and O_2 as oxidant at temperatures above 100 ºC can be written as

$$H_{2(g)} + 0.5O_{2(g)} \xrightarrow{Pt} 2H_2O_{(g)} \qquad \text{(R4)}$$

The maximum possible cell potential is achieved when the fuel cell is operated under the thermodynamically reversible condition. The fuel cell voltage is given from a combination of the thermodynamic cell potential and voltage losses associated with Ohmic resistances in the electrodes and membrane and kinetic losses at the anode and cathode which are influenced by mass transport restriction.

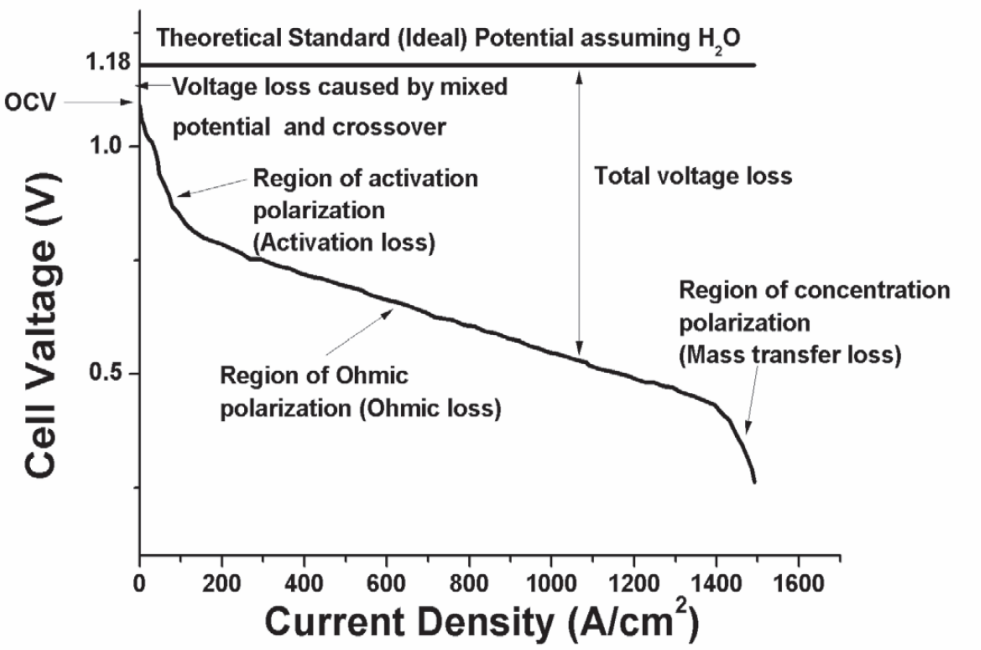

Figure 3.8 Typical polarization curve of PEMFCs (Jiang et al., 2011)

The overall reaction can be written as:

$$E_{\text{cell}} = E_{\text{rev}} - \eta_{\text{act}} - \eta_{\text{ohmic}} - \eta_{\text{conc}} \tag{6}$$

The Nernst equation can be used to calculate the reversible cell equilibrium, that E_{rev} is the maximum voltage.

$$E_{\text{rev}} = -\left(\frac{\Delta H_{\text{T}}}{nF} - \frac{T\Delta S_{\text{T}}}{nF}\right) + \frac{RT}{nF}\ln\left(\frac{(RT)^{1.5} C_{\text{H}_2\text{-Pt}} C_{\text{O}_2\text{-Pt}}^{0.5}}{a_{\text{H}_2\text{O}}}\right) \tag{7}$$

Where C_{Pt} is the concentration at the catalyst surface of the species i. F is the Faraday constant. ΔH_{T} and ΔS_{T} are the enthalpy and entropy, respectively.

$$\Delta S_{\mathrm{T}}\left(\mathrm{JK}^{-1}\right) = -9967.35\ln\left(T\right) + 12414.83 \tag{8}$$

The enthalpy of water formation in the gaseous phase can be written accordingly

$$\Delta H_{\mathrm{T}}\left(\mathrm{kJ}\right) = -238.41 - 0.012256T + 2.7656\times10^{-6}T^{2} \tag{9}$$

The water activity in the thin film is defined by the ratio of water partial pressure to its saturation pressure which is given by

$$a_{\mathrm{H_2O}} = \frac{P_{\mathrm{H_2O}}}{P^{*}_{\mathrm{H_2O}}} = \frac{\%RH}{100} \tag{10}$$

Steam tables and a polynomial function are used to determine saturated water vapour pressures in the temperature range of 273-500 K.

$$P^{\mathrm{sat*}}_{\mathrm{H_2O}} = \begin{pmatrix} 142.07682T^{4} - 171026.12676T^{3} + 78013638.11584T^{2} \\ -15953375633.8471T + 1231888491801.45 \end{pmatrix} \times 10^{-10} \tag{11}$$

3.3.1.1 Voltage losses

The voltage fluctuations during constant current operation as a function of parallel microchannels and the air flow rate stoichiometric ratio. Voltage loss in an operational fuel cell are explained by

Activation loss

At low current density, activation loss or activation polarization dominates losses which is the voltage potential required to overcome the activation energy of the electrochemical reaction on the catalyst surface. The Butler-Volmer equation applies to all single-step reactions, and some modifications to the equation must be made in order

to use it for multistep approximations. The Butler-Volmer equation can be also written as:

$$i_{\mathrm{a}} = i_{0,\mathrm{a}}\left(\exp\left(\frac{-\alpha_{\mathrm{Rd,a}}F}{RT}(\eta_{\mathrm{a}})\right) - \exp\left(\frac{-\alpha_{\mathrm{Ox,a}}F}{RT}(\eta_{\mathrm{a}})\right)\right) \tag{12}$$

$$i_{\mathrm{c}} = i_{0,\mathrm{c}}\left(\exp\left(\frac{-\alpha_{\mathrm{Rd,c}}F}{RT}(\eta_{\mathrm{c}})\right) - \exp\left(\frac{-\alpha_{\mathrm{Ox,c}}F}{RT}(\eta_{\mathrm{c}})\right)\right) \tag{13}$$

Where i is the exchange current density and α is a transfer coefficient. i_0 is exchange current density which can be calculated by

$$i_0 = i_0^{\mathrm{ref}} a_c L_c \left(\frac{C_{\mathrm{Pt}}}{C_{\mathrm{Pt}}^{\mathrm{ref}}}\right)^{\gamma} \exp\left[-\frac{E_{\mathrm{c}}}{RT}\left(1-\frac{T}{T_{\mathrm{ref}}}\right)\right] \tag{14}$$

Where i_0^{ref} is the current density which is measured at a reference temperature T_{ref} and reference dissolved reactant concentration is $C_{\mathrm{Pt}}^{\mathrm{ref}}$. E_{c} is the activation energy. L_c and a_c are the catalyst loading and the catalyst specific accessible electrochemical surface area, respectively. The major advantage of HT-PEMFCs is the CO tolerance and the system has the ability to operate with reformate gas fee without considerable loss in performance. Therefore, the CO poisoning effect on the anode activation loss of the HT-PEMFC can be neglected. Shamardina et al. 2010 purpose that the Tafel equation can be used to calculate the cathode activation loss, as shown as below:

$$i = i_0\left(\frac{C_{O_2}}{C_{ref}}\right)\exp\left(\frac{\eta_{act}}{b}\right) \tag{15}$$

Where i is the exchange current density, C_{O_2} is the oxygen concentration, C_{ref} is the reference concentration, η_{act} is the cathode activation loss and b is the Tafel slope which can be calculated by:

$$b = \frac{RT}{\alpha F} \tag{16}$$

Where R is gas constant, T is the cell temperature, α is the transfer coefficient and F is the Faraday's constant.

Ohmic loss

The ohmic loss is caused by charge transport resistance in the electrolyte through membrane. The flow of ions through the electrically conductive fuel cell components can be cause of voltage drop. It can be calculated by the correlation base on a PEM fuel cell using a PBI membrane which is purposed by Cheddie et al. 2006

$$\eta_{ohmic} = i\left(\frac{l_m}{\kappa_m} + \frac{l_d}{\sigma_d}\right) \tag{17}$$

Where l_m is the thickness of membrane, κ_m is the ion conductivity, l_d is the thickness of GDL and σ_d is the electrical conductivity of the gas diffusion electrode.

Concentration losses

At high current density, the concentration of reactants on catalyst layer are consumed rapidly by electrochemical reaction. Thus the electrode is controlled by mass transfer of oxygen. The mass transport losses or concentration losses can be calculated by:

$$\eta_{conc} = \frac{RT}{nF} \ln\left(\frac{i_L}{i_L - i}\right) \tag{18}$$

Where i_L is the limiting current density which the reactant concentration reaches to zero at this operating current density. The limiting current density bases on the oxygen transfer:

$$i_L = \frac{4FD_{O_2}^{eff} C_{O_2}}{l_d} \tag{19}$$

Where $D_{O_2}^{eff}$ is the effective oxygen diffusivity and C_{O_2} is the concentration of oxygen at the channel inlet.

As mentioned, the fuel cell is used to convert chemical energy to electrical energy. The electrical power output of fuel cell can be calculated from current density and cell voltage (E_{cell}), as shown as:

$$P_{FC} = iE_{\text{cell}} \tag{20}$$

3.4 Exergy Analysis

Exergy is defined as the maximum work which can be obtained from a system during a process that brings the system at general state (T,P) into equilibrium at reference state (T_0,P_0) (Hajjaji et al., 2012). The concept of exergy analysis is based on the second law of thermodynamics which can identify the causes, location and magnitudes of process inefficiencies.

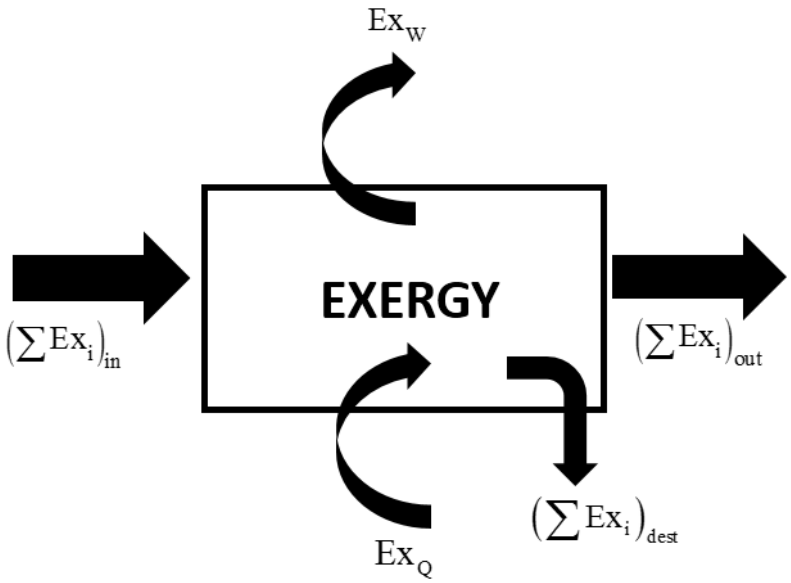

Figure 3.9 Exergy balance on the system

The overall exergy equation can be written for steady-state process as follows

$$\left(\sum Ex_i\right)_{in} = \left(\sum Ex_j\right)_{out} + \left(\sum Ex\right)_{dest} \quad (21)$$

Where $\left(\sum Ex_i\right)_{in}$ is the total energy input, $\left(\sum Ex_j\right)_{out}$ is the total energy output and $\left(\sum Ex\right)_{dest}$ is the destruction rates.

The exergy of thermal energy associated with heat transfer depends on temperature and heat of system is given by

$$Ex_Q = Q\left(1 - \frac{T_0}{T}\right) \quad (22)$$

where Q is the amount of heat transferred, T_0 is the reference temperature, and T is the temperature at which the heat transfer occurs.

The exergy associated with an exchange of mechanical work is

$$Ex_W = W \quad (23)$$

Typically, the exergy of system is the sum of thermomechanical exergy, chemical exergy, kinetic exergy and potential exergy. However, kinetic exergy and potential exergy are very small compared with chemical exergy and thermomechanical exergy in this work. Therefore, the exergy of the flowing stream are only divided into two parts: physical exergy and chemical exergy as shown in

$$ex_{total} = ex_{ph} + ex_{ch} \quad (24)$$

where ex_{ph} is the physical exergy which is the maximum useful work obtained by passing the unit of mass of substance of the generic state (T, P) to the reference state (T_0, P_0). The physical exergy can be calculated by

$$ex_{ph} = (h - h_0) - T_0(s - s_0) \quad (25)$$

The chemical exergy (Ex_{ch}) is the maximum amount of work obtainable when the substance under consideration is brought from the environment state (T_0, P_0) to the reference state. It can be express by

$$ex_{ch} = \sum_{i=1}^{n_{species}} x_i \cdot ex_{i,ch}^{0} + RT_0 \sum_{i=1}^{n_{species}} x_i \cdot \ln(x_i) \quad (26)$$

where $ex_{i,ch}^{0}$ is the standard chemical exergy of component i and x_i is the mole fraction.

CHAPTER IV
Modeling of SECLR process and HT-PEMFC

This chapter explains description of sorption enhance chemical reforming (SECLR) process simulation in Aspen Plus. In addition, the simulation of high temperature proton exchange membrane is described in the next section. The SECLR and HT-PEMFC integrated system consists of fuel reactor, calcination reactor, air reactor and HT-PEMFC stack. SECLR process converts biogas to H_2-rich gas, and then this gas is used as fuels of HT-PEMFC to generate electric power. This study aims to analyze the SECLR and HT-PEMFC integrated system. Firstly, the SECLR process and HT-PEMFC which are developed is validated with data reported in the literatures. Then, the SECLR process is investigated the effect of operating conditions to find suitable operating conditions. Finally, the system efficiency of integrated system is determined.

4.1 SECLR simulation

For chemical plant design, the simulation software is used for the design, development and optimization of processes. The simulators can help engineer predict the behavior of a process system. At present, there are many chemical process simulators such as Aspen Plus, Aspen HYSYS, CHEMCAD and others. Aspen Plus is the most popular process simulation software programs used academically and industrially. Because it has various thermodynamic properties for many common substances and unit modules. Moreover, the user can create new modules which doesn't have in Aspen Plus.

The aim of SECLR process simulation is to investigate the characteristics of SECLR process to generate hydrogen from biogas.

4.1.1 Selection of thermodynamic method

The first of process simulation in Aspen Plus is the thermodynamic method selection. Because the incorrect calculation can be caused by the improper thermodynamic method. The thermodynamic method is used to calculate properties such as K-values, enthalpy and density. This study selects a property method base on 'SOLIDS' property method in the simulation because the physical property for solids are different from the conventional properties for fluid. Solid property method is concerned with type of substream which is explained in 4.1.3.

4.1.2 Specification of components

In a term of reaction, multiple reactions which include partial and complete oxidation of the fuel take place in the fuel reactor of a SECLR process. In this study, all reactors of SECLR process are operated at steady state, isothermal and isobaric conditions. In the flowsheet simulator, the minimization of Gibbs free energy is used to calculate the composition of the gaseous products. The feedstock of SECLR process is biogas which its composition is shown in Table 4.2.

Table 4.1 Reaction involved in SECLR process (A. Lima da Silva et al., 2012).

Fuel reactor (FR)		
Oxygen carrier reductions	$CH_4 + 4NiO \rightarrow 4Ni + CO_2 + 2H_2O$	ΔH^o_{298K} = 156 kJ/mol
	$H_2 + NiO \rightarrow Ni + H_2O$	ΔH^o_{298K} = -2.1 kJ/mol
	$CO + NiO \rightarrow Ni + CO_2$	ΔH^o_{298K} = -43.3 kJ/mol
	$C + NiO \rightarrow Ni + CO$	ΔH^o_{298K} = 129.2 kJ/mol
	$CH_4 + NiO \rightarrow Ni + CO + 2H_2$	ΔH^o_{298K} = 169.9 kJ/mol
Steam reforming	$CH_4 + H_2O \rightarrow CO + 3H_2$	ΔH^o_{298K} = 205.8 kJ/mol
Dry reforming	$CH_4 + CO_2 \rightarrow 2CO + 2H_2$	ΔH^o_{298K} = 247 kJ/mol
Methane decomposition	$CH_4 \rightarrow C + 2H_2$	ΔH^o_{298K} = 74.5 kJ/mol
Carbon gasification	$C + H_2O \rightarrow CO + H_2$	ΔH^o_{298K} = 131.3 kJ/mol
Boudouard	$2CO \rightarrow C + CO_2$	ΔH^o_{298K} = -172 kJ/mol
Combustion	$CH_4 + 2O_2 \rightarrow CO_2 + 2H_2O$	ΔH^o_{298K} = -806 kJ/mol
Water-gas shift	$CO + H_2O \rightarrow CO_2 + H_2$	ΔH^o_{298K} = -41.2 kJ/mol
Carbonation	$CaO + CO_2 \rightarrow CaCO_3$	ΔH^o_{298K} = -178.8 kJ/mol
Calcinator (CAL)		
Calcination	$CaCO_3 \rightarrow CaO + CO_2$	ΔH^o_{298K} = 178 kJ/mol
Air reactor (AR)		
Oxygen carrier oxidation	$Ni + 0.5O_2 + 1.881N_2 \rightarrow NiO + 1.881N_2$	ΔH^o_{298K} = -239 kJ/mol

In a term of simulation, the SECLR process is investigated using reactant biogas from the anaerobic digestion of the landfill material. The molar composition of landfill biogas is shown in Table 4.2.

Table 4.2 Biogas molar compositions (Gopaul et al., 2015).

Component	kmol/hr
CH_4	0.50
CO_2	0.35
O_2	0.03
N_2	0.13
H_2	0
Total	1

For simulation of SECLR process by Aspen plus, all components are specified as shown in Table 4.3.

Table 4.3 Specification components.

Component name	Type
Methane	Conventional
Water	Conventional
Hydrogen	Conventional
Carbondioxide	Conventional
Carbonmonoxide	Conventional
Nitrogen	Conventional
Oxygen	Conventional
Calciumoxide	Solid
Calciumcarbonate	Solid
Nickel	Solid
Nickeloxide	Solid
Carbon	Solid

4.1.3 Setup for simulation

This process contains solid particles such as NiO and CaO. Therefore, the suitable physical property is required for the solid process. Then, the solids simulation can be selected in this work. Typically, the most simulation are conventional process which contains only liquid and gas. For this reason, the configuration of simulation is setup a stream class as MIXCIPSD for solids and gases separation.

4.1.4 SECLR flow sheet configuration

The novel part of sorption enhanced chemical-looping reforming (SECLR) process involves three interconnected reactors. Therefore, modeling SECLR process in Aspen Plus model is divided into three reactors including of a fuel reactor 'FR', a calcination reactor 'CAL' and an air reactor 'AR'. Three cyclones, 'CYC1', 'CYC2' and 'CYC3' are used to separate the Ni and $CaCO_3$ solid from gases. In this simulation, there are six heat exchangers which are used for heating and cooling the feed stream. Figure 4.1 shows flow sheet of SECLR process.

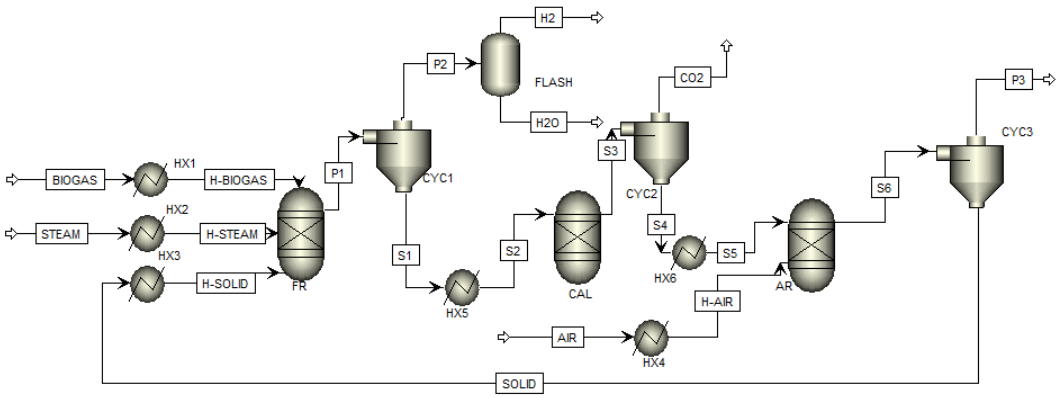

Figure 4.1 Flowsheet of SECLR simulation.

A SECLR process mostly carry out in fluidized bed reactors. For simulation in Aspen Plus, equilibrium RGIBBs reactors which are the calculation of chemical and phase equilibrium using Gibbs free energy minimization are used as the fluidized bed reactors. They are analyzed at steady state operation with isobaric and isothermal conditions. The process is operated at 1 atm. The reactant feed streams are divided in two streams which are 'BIOGAS' and 'STEAM'. They are preheated to a temperature of fuel reactor at 1 atm and then enter to fuel reactor block, 'FR'. In this process, the regeneration solid NiO and CaO are fed simultaneously to fuel reactor. In a fuel reactor, fuel is oxidized with NiO, H_2O and CO_2. The block 'CAL' is used to convert the $CaCO_3$ to CaO for regeneration. The products of each reactor are separated gas and solid by cyclone. The solid products of calcination reactor, 'CAL' are sent to air reactor, 'AR' for NiO regeneration. In term of H_2 rich gas, Flash drum module 'FLASH' is used to separate steam from the hydrogen rich gas product which is produced by fuel reactor. The hydrogen product stream 'H_2' is analyzed in dry basis composition. Then, these modules are used to simulate the SECLR process. The process description is shown in Table 4.4.

Table 4.4 Process description

Module	Component	Description
FR	Fuel reactor	Simulate steam reforming and oxidation reactions
CAL	Calcination reactor	Simulate the regeneration of CaO by calcination reaction
AR	Air reactor	Simulate the regeneration of NiO by oxidation reaction
Flash	Flash	To remove H_2O from syngas product
CYC1	Cyclone	Separate solid and gas products form fuel reactor
CYC2	Cyclone	Separate solid and gas products form calcination reactor
CYC3	Cyclone	Separate solid and gas products form air reactor
HX1	Heater	To preheat biogas
HX2	Heater	To preheat steam
HX3	Heater	To cool solid
HX4	Heater	To preheat air
HX5	Heater	To preheat $CaCO_3$ and Ni
HX6	Heater	To preheat CaO and Ni

4.2 HT-PEMFCs simulation

In a term of HT–PEMFC stack modeling, the stack which is simulated by Aspen Plus software is separated into two part, anode and cathode. The H_2-rich gas stream 'H2' is preheated, and then fed to the block 'Anode' which is simulated by separator to provide hydrogen for electrochemical reaction. A certain amount of hydrogen is separated is separated in the 'ANODE' block and enter to 'CATHODE' block to react with oxygen. The anode-off gas stream 'AOG' feds to the afterburner 'AFB' to combust with air to produce additional heat. The anode fuel equivalent hydrogen molar flowrate is calculated base on the fuel utilization factor.

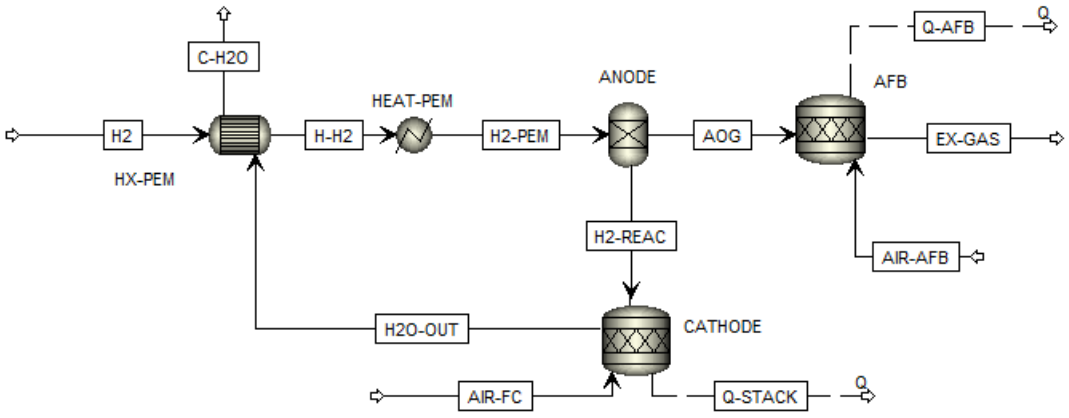

Figure 4.2 Flowsheet of HT-PEMFC simulation

The values of parameters which are used in HT-PEMFC modelling are shown in table 4.5. They are imported form experimental data of Shamardina et al. (2010). The electrochemical calculation need for these parameters which are shown in Table 4.5.

Table 4.5 The values of the parameters used for HT-PEMFC modelling (Shammardina et al., 2010).

Parameters	Values
Fuel cell temperatures, T(ºC)	160
Faraday constant, F (C mol^{-1})	96485
Gas constant, R (J mol^{-1} K^{-1})	8.314
Operating pressure at anode, P (atm)	1
Operating pressure at Cathode, P (atm)	1
Reference concentration, C_{ref} (mol cm^{-3})	$2.8x10^{-5}$
Thickness of the GDL, l_d (cm)	0.04
Thickness of the membrane, l_m (cm)	0.006
Electrical conductivity of the gas diffusion electrode, σ_d (S cm^{-1})	2.2
Ionic conductivity, κ_m (Km)	0.038
Transfer coefficient, α	0.8

4.3 Model Validation

The model of the SECLR process and HT-PEMFC which mentioned in the previous section are confirmed by the result of the validation between simulation and experimental data in the same condition.

The simulation of SECLR process using the developed flowsheeting model is performed and validated against the experimental data of Rydén and Ramos (2012). In experiment, they use pure methane as a fuel of hydrogen production process. In a term of model as function of temperature, the fraction of H_2 in the reforming gas is predicted

by the developed flowsheeting model under the same operating conditions (steam to carbon ratio of 1.8, NiO to carbon ratio of 1 and CaO to carbon ration of 1). The results from this simulation are compare with the experimental data as shown in Figure 4.3. The simulation results obtained from equilibrium composition could not be expected to fit perfectly with the experimental data because the mole of oxygen carrier in the reforming reaction may slightly vary during the reduction period. Moreover, the actual reformate gas should have a higher H/C ratio than the equilibrium conditions. The deviation of simulation results are shown in Table 4.6.

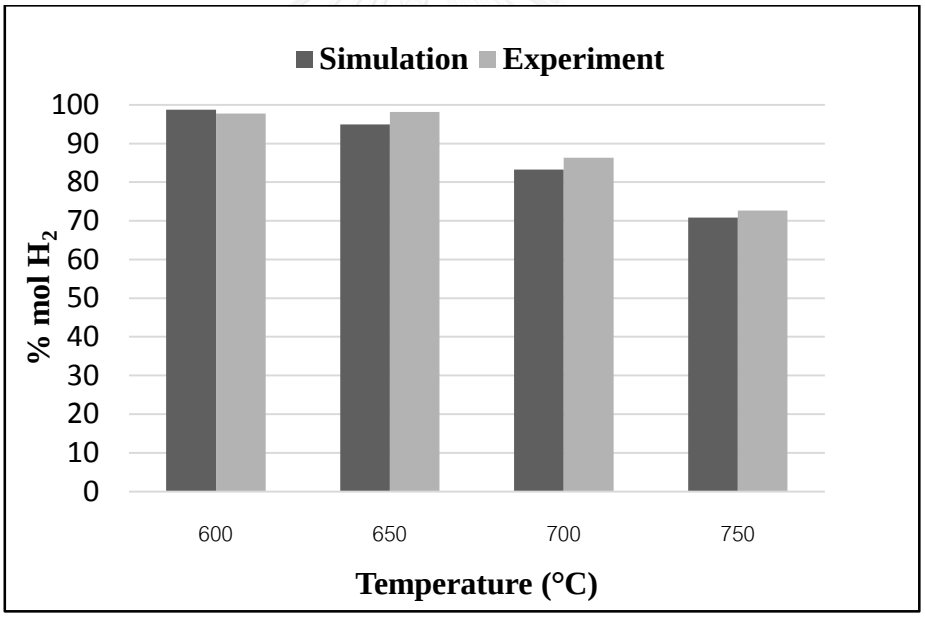

Figure 4.3 Comparison of model prediction and experimental data of Rydén and Ramos (2012)

Table 4.6 Comparison of simulation data and experimental data.

Reforming temperature (ºC)	H_2 mole fraction (Simulation) (%)	H_2 mole fraction (Experiment) (%)	Simulation error (%)
600	98.79	97.73	1.08
650	94.96	98.18	3.28
700	83.31	86.36	3.53
750	70.86	72.63	2.44

Figure 4.4 shows the generation of CO_2 from simulation reasonably fit with the experimental data. Therefore, this model can be used for SECLR process analysis. The simulation deviation are shown in Table 4.7.

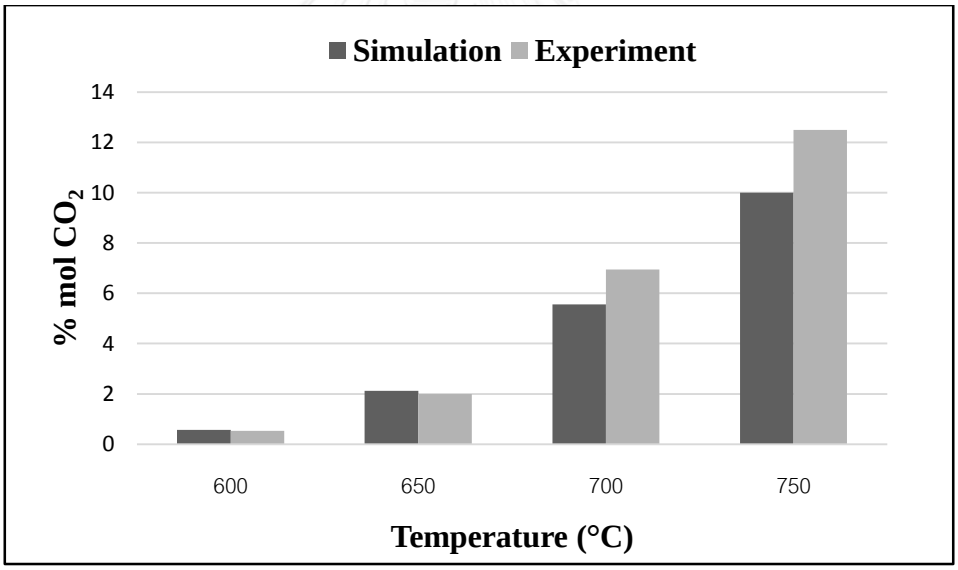

Figure 4.4 Comparison of model prediction and experimental data of Rydén and Ramos (2012)

Table 4.7 Comparison of simulation data and experimental data.

Reforming temperature (ºC)	CO_2 mole fraction (Simulation) (%)	CO_2 mole fraction (Experiment) (%)	Simulation error (%)
600	0.57	0.53	7.01
650	2.12	2.00	12.00
700	5.56	6.95	20.00
750	10.00	12.50	20.00

The HT-PEMFC stack which is implemented in this study is the steady-state electrochemical model. The results of HT-PEMFC model are compared with the experiment of Shamardina et al. (2010). The experiment of HT-PEM is operated at temperature of 160 ºC, pressure of 1 atm and N_2 to O_2 mole ratio of 0.79/0.21. In a term of polarization curve, Fig 4.5 shows that the model predictions are good agreement with the experimental data.

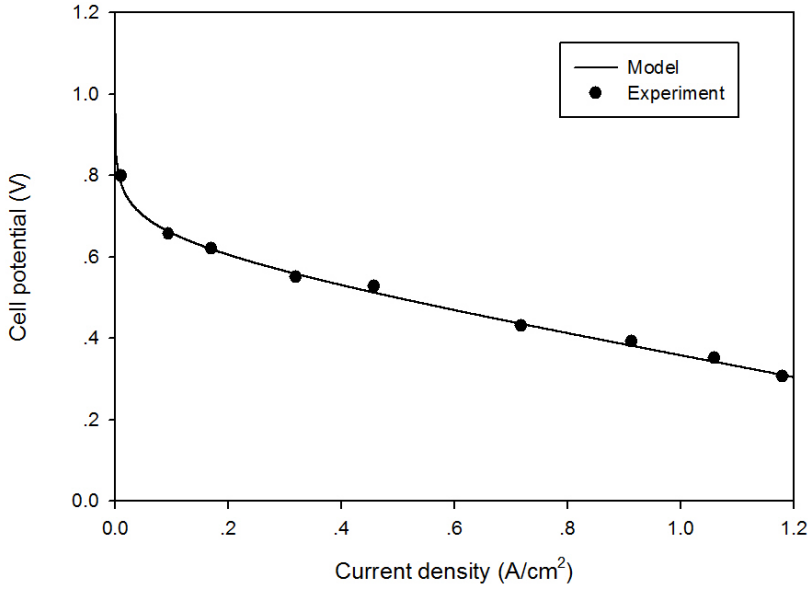

Figure 4.5 Comparison between modelled and experimental polarization curve.

CHAPTER V

Thermodynamic analysis of a SECLR process for hydrogen production

The aim of this chapter is to thermodynamically analyze the sorption enhance chemical looping reforming (SECLR) of biogas for hydrogen production, and compare with previous chemical looping reforming process (CLR), which has no CO_2 capture. The proposed methodology for thermodynamic calculation is the minimizing Gibbs free energy that can guarantees the global optimum acquisition without the necessity of initial estimates. It used to provide the information on operating parameters such as fuel reactor temperature and feed compositions. Because the high hydrogen yield and purity can be obtained from the suitable operating conditions. Furthermore, they can be a new approach to reduce the energy consumption in the process.

5.1 Analysis of operating parameters

A sensitivity analysis can provide information on the degree to which a design parameter must be changed in order to achieve a desired product quality. The results of parametric analysis are expressed in term of yield and purity of product H_2 on dry basis**.** In a term of energy balance, the previous studies show that the amount of feed stream such as NiO, steam and air change can be caused by the net energy decreasing. Therefore, heat duty for each unit is considered for a part of process improvement.

$$Yield\ of\ H_2 = \frac{\dot{n}_{H_2,out}}{\dot{n}_{Biogas,\ feed}} \tag{27}$$

$$\%\ \text{Purity of } H_2\left(\text{Dry basis}\right) = \frac{\dot{n}_{H_2,out}}{\dot{n}_{total,out} - \dot{n}_{H_2O,out}} \times 100\% \quad (28)$$

$$\text{NiO/B} = \frac{\dot{n}_{NiO}}{\dot{n}_{Biogas}} \quad (29)$$

$$\text{S/B} = \frac{\dot{n}_{H_2O}}{\dot{n}_{Biogas}} \quad (30)$$

$$\text{CaO/B} = \frac{\dot{n}_{CaO}}{\dot{n}_{Biogas}} \quad (31)$$

$$\text{Air/B} = \frac{\dot{n}_{Air}}{\dot{n}_{Biogas}} \quad (32)$$

Where $\dot{n}_i$ is the molar flowrate of specie i.

5.2 Results and discussion

5.2.1 CO_2 capture effect on chemical looping reforming process

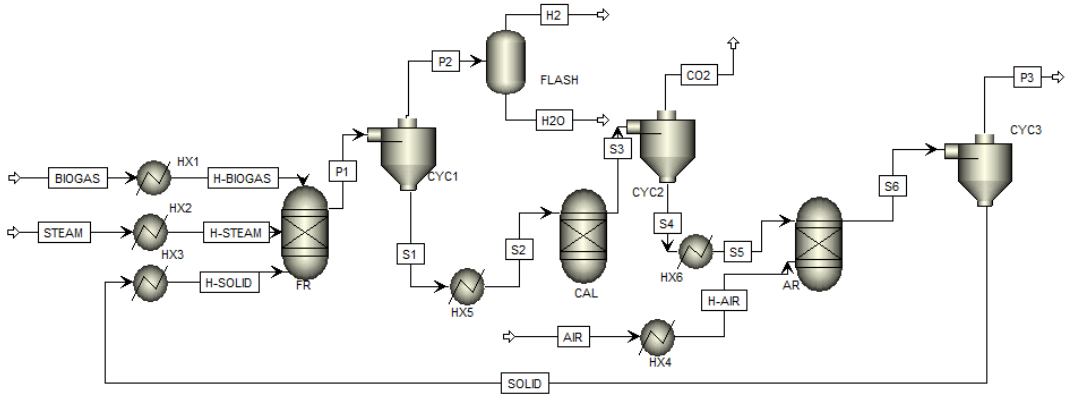

Figure 5.1 Schemetic description of SECLR process

Chemical looping reforming (CLR) without CaO looping and sorption enhanced chemical looping reforming (SECLR) process are compared by investigating CO_2 capture in the process illustrated in Figure 5.1. In a part of simulation, the both of CLR and SECLR are operated at the same conditions. The reactants is preheated equal the temperature of the reforming reactor. The fuel reactor temperature is varied from 500 °C to 800 °C at 1 atm. In addition, the concentration of CO is consider in this simulation because CO poisons the catalyst of HT-PEMFC. The results of simulation are shown in Table 5.1.

Table 5.1 Comparison of hydrogen purity of CLR process and SECLR process

T_{FR} (C)	**%H_2 (SECLR)**	**%H_2 (CLR)**	**%CO (SECLR)**	**%CO (CLR)**
500	87.49	36.54	0.01	4.03
600	86.75	48.69	0.48	11.20
700	74.31	50.64	0.07	16.52
800	49.52	49.52	0.2	19.99

Although the HT-PEMFC can tolerate up to 3% CO, the higher stack power can be obtained at the low concentration of CO. The benefit of CO_2 capture is the increasing of H_2 purity and reduction of CO poisons at lower temperature.

From table 5.1, the results show that the SECLR process can obtain higher hydrogen purity that the CLR process because the CO_2 capturing by CaO can shift equilibrium forward which can promote hydrogen yield via stream reforming reaction.

As mentioned, the higher H_2 yield and H_2 purity can be achieved by increasing steam and adding the CaO sorbent.

5.2.2 Effect of steam-to-biogas molar ratio (S/B) and reforming temperature

In this case, the simulation investigates the effect of steam-to-biogas molar ratio (S/B) with varying the operating temperature at a biogas 1 kmol/hr, NiO/B ratio of 0.5 and CaO/B ratio of 1. The simulation results show that the hydrogen purity and yield increase with increasing S/B ratio, as illustrated in Figure 5.2 and 5.3, respectively. Because the increasing steam can shift the equilibrium compositions of the steam reforming reaction. The effect of operating temperature on hydrogen purity and yield are investigated. The results indicate that the highest hydrogen purity can be achieved at high S/B ratio and 500 ºC, as illustrated in Figure 5.2.

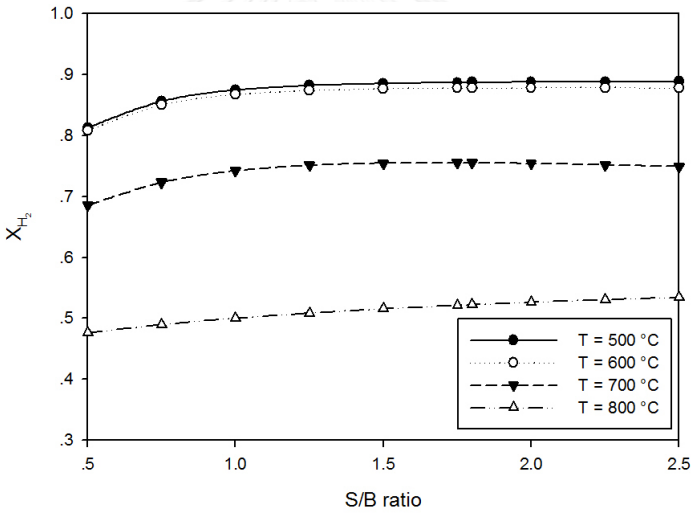

Figure 5.2 Effect of S/B ratio on mole fraction of hydrogen with dry basis at NiO/B ratio of 0.5, CaO/B ratio of 1 and different temperature.

Figure 5.3 shows that the highest hydrogen yield can be obtained at 600 ºC in the S/B molar ratio range of 0.75-1.25. The increasing of S/B molar ratio that can produce more hydrogen yield and hydrogen purity because the equilibrium of steam reforming reaction and water gas shift reaction are promoted due to shifting the equilibrium compositions. However, the S/B molar ratios are greater than 1.5, the

highest hydrogen production yield can be achieved at 500 ºC. In term of reforming temperature, the high hydrogen yield can be obtained with low reforming temperature 500-600 ºC because the CO_2 adsorption is occurred at low temperature due to the exothermic adsorption. The CO_2 capture can shift the equilibrium composition to right that promotes the hydrogen production.

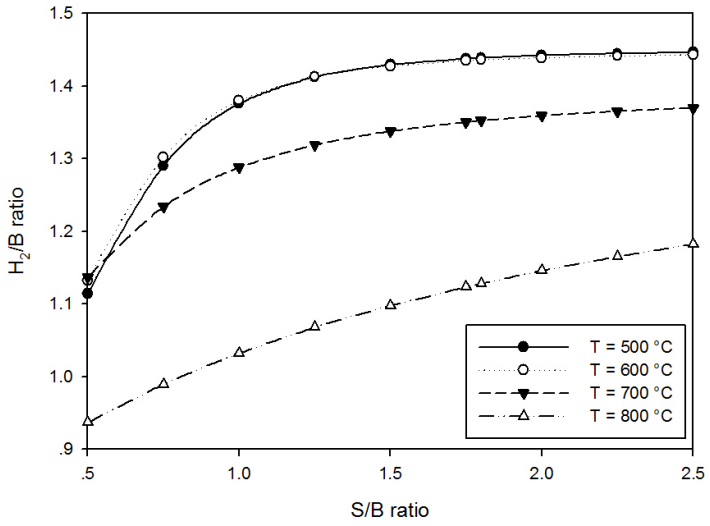

Figure 5.3 Effect of S/B ratio on hydrogen yield at NiO/B ratio of 0.5, CaO/B ratio of 1 and different temperature.

5.2.3 Effect of nickel oxide-to-biogas molar ratio (NiO/B) and reforming temperature on hydrogen purity and yield.

Although partial oxidation of CH_4 with NiO is endothermic reaction, a suitable amount of NiO addition can provide heat for a process due to oxidation of Ni with air in air reactor. It can be used as energy carrier for reforming reactor. However, the increasing of NiO/B ratio decreases the hydrogen yield and purity because hydrogen is converted to water by oxygen carrier reduction. Therefore, the effect of NiO/B ratio on hydrogen purity and yield is investigated. Figure 5.4 shows that the simulation is carried out at S/B ratio of 2 and CaO/B of 1. The result shows that the highest hydrogen purity

is achieved at low reforming temperature 500 ºC. The increasing of NiO/biogas ratio decreases the hydrogen yield and purity because the partial oxidation reaction is changed to complete oxidation reaction with high content of oxygen carrier. Thus, the content of oxygen carrier must be prevented in the partial oxidation condition.

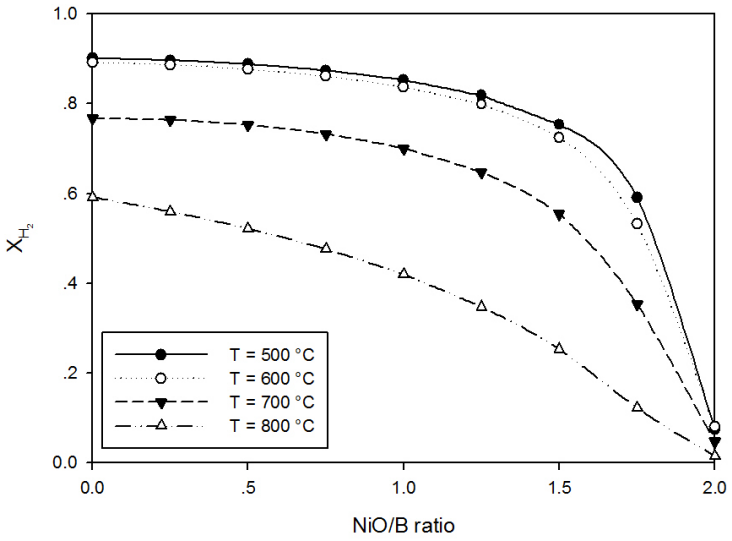

Figure 5.4 Effect of NiO/B ratio on mole fraction of hydrogen with dry basis at S/B ratio of 2, CaO/B ratio of 1 and different temperature.

In addition, the result of effect of temperature on H_2/B yield shows that the highest hydrogen production yield is obtained with low temperature 500 ºC, as shown in Figure 5.5.

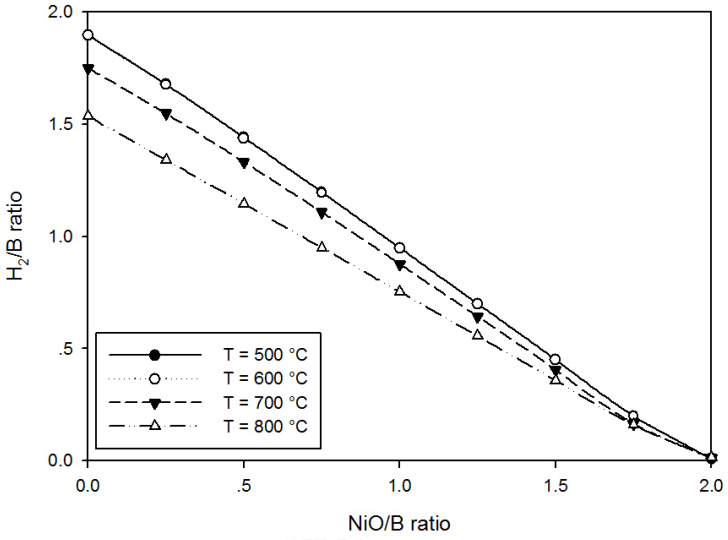

Figure 5.5 Effect of NiO/B ratio on hydrogen yield at S/B ratio of 2, CaO/B ratio of 1 and different temperature.

5.2.4 Effect of nickel oxide-to-biogas molar ratio (NiO/B) on the concentration of CO in reformate gas

For SECLR integrated with HT-PEMFC system, the concentration of CO in reformate gas must be considered due to CO poisoning on Pt catalyst. Therefore, NiO can be the effective way to reduce CO content in reformate gas because NiO can convert CO to CO_2 by NiO reduction. Figure 5.6 show the effect of NiO on CO content in reformate gas. The concentration of CO is decreased with increasing of NiO/B ratio and it is near to zero at NiO/B molar ratio near 2. In addition, the CO content can be affected by reforming temperature. The result show that the reforming temperature at 500-600 ºC can reduce the concentration of CO near close to zero.

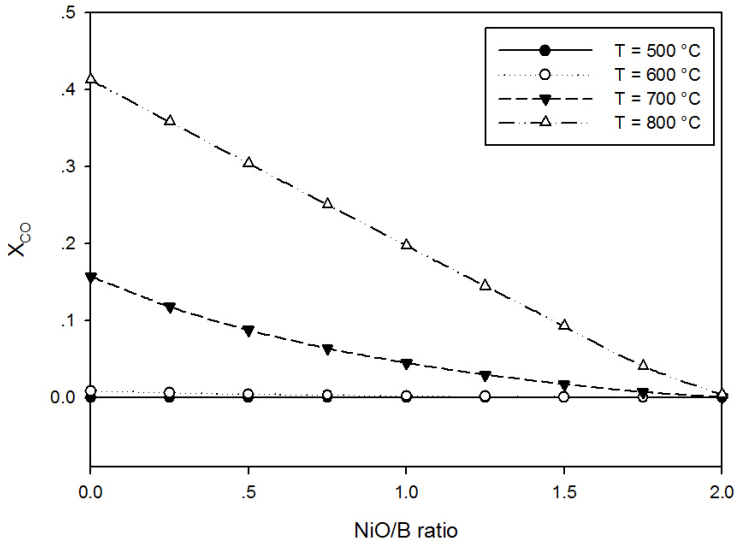

Figure 5.6 Effect of NiO/B ratio on mole fraction of carbonmonoxide with dry basis at S/B ratio of 2, CaO/B ratio of 1 and different temperature.

5.2.5 Effect of nickel oxide-to-biogas molar ratio (NiO/B) on the net energy demand for the SECLR process

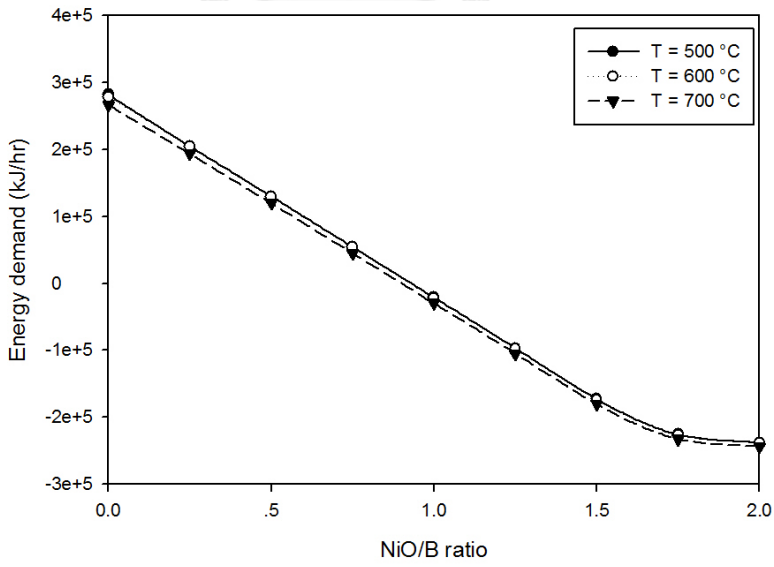

Figure 5.7 Effect of NiO/B ratio on the net energy of SECLR process at S/B ratio of 2, CaO/B ratio of 1 and different temperature.

To investigate energy balance of this system, the process is simulated at fuel reactor temperature 500-700 ºC, S/B ratio of 2 and CaO/B ratio of 1. The effect of NiO/B ratio on net energy of SECLR process shows that the net heat duty is increased with increasing reforming temperature. In term of NiO/B ratio, the total net energy requirement for overall process that needs to operate this system is decreased with increasing amount of NiO due to exothermic reaction in air reactor which is used to convert Ni to NiO for regeneration, as shown in Figure 5.7. Therefore, the increasing of NiO/B ratio can reach to autothermal operating condition. However, the effect of NiO/B ratio on hydrogen yield and purity is still considered due to using in fuel cell integration. Moreover, the effect of S/B ratio and NiO/B ratio must be considered simultaneously because the amount of fed stream can increase energy to preheat steam for fuel reactor and increase hydrogen production while NiO/B is improving energy balance in the system. However, this part can't conclude that the energy consumption in this process is suitable because the next part is integrated with HT-PEMFC which can produce heat from exothermic electrochemical reaction to supply the reforming process. Therefore, the thermal efficiency of SECLR process is investigated in the next chapter.

5.2.6 Carbon formation in a SECLR process

A major problem in the reforming process is the carbon formation or carbon deposition. It can be occurred by side reactions such as Boudouard reaction or methane cracking. Therefore, the way to reduce the risk of carbon formation must be investigated. Figure 5.8 show that amount of carbon formation occurs with different

CaO/B and S/B. The carbon free region at S/B ratio of 2.0 and 500 ºC can be obtain at CaO/B ratio more than 0.65. They can be used as initial condition to analyze other parameter with free carbon.

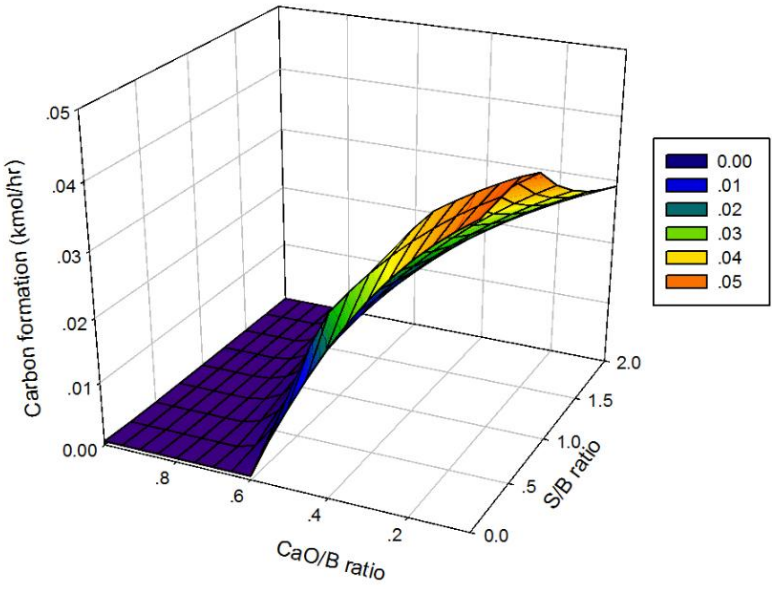

Figure 5.8 Effect of CaO/B ratio and S/B ratio on the amount of carbon formation at NiO/B ratio of 0.5 and 500 ºC.

The effect of S/B ratio on amount of carbon formation is investigated because the carbon gasification reaction can convert carbon to CO and H_2. Moreover, the carbon formation can be occurred by the operating temperature which can occur Boudouard reaction. Therefore, the amount of carbon formation with varying S/B ratio and reforming temperature is shown in Figure 5.9. The result show that the carbon formation is occurred with S/B ratio near 0 at temperature exceeding 500 ºC. However, this process is examined with S/B ratio more than 0.5 which can ensure that the carbon formation is not occurred.

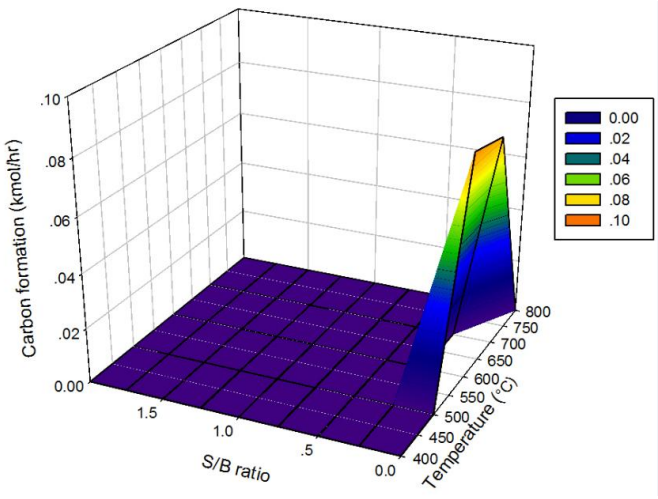

Figure 5.9 Effect of S/B ratio and reforming temperature on the amount of carbon formation at NiO/B ratio of 0.5 and CaO/B of 1.

5.2.7 Effect of nickel oxide-to-biogas molar ratio (NiO/B) and calcium oxide-to-biogas molar ratio (CaO/B) on the SECLR process

As mentioned, the role of NiO is to provide heat required to the system and reduce concentration of CO in reformate gas. However, the use of NiO as an oxygen carrier in SECLR process increases amount of CO_2 in reforming gas. In this study, CaO which is used as CO_2 capture is considered. Figure 5.10 shows the effect CaO/B ratio on hydrogen purity with varying NiO/B ratio. It can be seen that the increasing of CaO/B ratio achieved more hydrogen purity. The maximum hydrogen purity is obtained at CaO/B ratio of 0.85. When the CaO/B ratio is greater than 0.85, the hydrogen purity does not change because there is no CO_2 in system to capture.

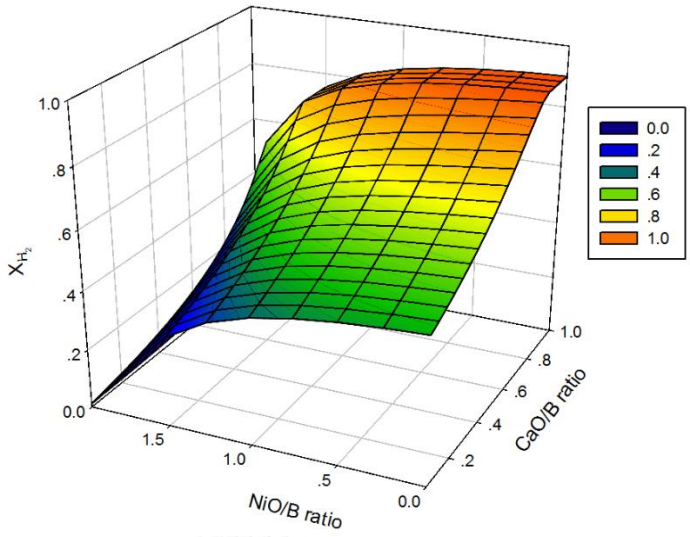

Figure 5.10 Effect of NiO/B ratio and CaO/B ratio on mole fraction of hydrogen at S/B ratio of 2 and 500 ºC.

5.3 Conclusion

At mentioned, the result show that the CO_2 capture using CaO can increases the hydrogen yield and purity of the SECLR process. Moreover, the CO contamination in reformate can be reduced by CO_2 capture. Furthermore, it can be observed that the increasing of S/B ratio increases the hydrogen yield and purity. However, the process needs more external energy to supply when operates at high S/B ratio. In term of oxygen carrier, the increasing NiO/B ratio can reduce the external heat requirement. In contrast, the high NiO/B ratio decreases the hydrogen yield and purity.Therefore, the suitable S/B and NiO/B ratio do not conclude in this chapter. They are going to analyze in the term of energy and exergy efficiency in the next section.

CHAPTER VI

Energy analysis of a SECLR process and HT-PEMFC integrated system

In this study, the H_2-rich gas which is produced from biogas by SECLR process is used as a fuel for HT-PEMFC. Therefore, the performance of SECLR process and HT-PEMFC is analyzed in this chapter due to effect of reformate gas composition. For reformate gas used as anode fuels, its composition depend on the operating condition of biogas reforming process. Moreover, the amount of reactants in the system can also directly affect the output of HT-PEMFC.

6.1 Analysis of a SECLR process and HT-PEMFC integrated system

The HT-PEMFC efficiency and heat duty in the SECLR system can be affected by feed ratio and operating temperature. In this study, the water content in the reformate gas is separated at 25 ºC by flash drum. Firstly, the total energy used for SECLR process, lower heating value of H_2 $\left(\text{LHV}_{H_2}\right)$ and lower heating value of fuel $\left(\text{LHV}_{\text{biogas}}\right)$ are used to compute the efficiency of SECLR process by eq (6.1).

$$\eta_{\text{SECLR}}(\%) = \frac{\dot{m}_{H_2} \bullet \text{LHV}_{H_2}}{\dot{m}_{\text{biogas}} \bullet \text{LHV}_{\text{biogas}} + Q_{\text{net,input}}} \times 100\% \tag{33}$$

Where $\dot{m}_{H_2}$ is the molar flowrate of H_2, $\dot{m}_{\text{biogas}}$ is the molar flowrate of biogas and Q_{net} is the heat duty net input to the reforming system. In this study, the lower heating value

of biogas and hydrogen are 481.35 kJ/mol and 242 kJ/mol, respectively which are used in the efficiency calculation.

However, HT-PEMFC is typically operated at 160 ºC. Therefore, the reformate gas which is used as fuel needs to be heated to 160 ºC. The electric power density and lower heating value of H_2 $\left(LHV_{H_2}\right)$ are used to calculated the fuel cell efficiency by eq (6.1). In the previous section, the hydrogen yield and hydrogen purity are increased by the increasing of S/B ratio.

$$\eta_{FC}(\%)=\frac{P_{FC}\bullet U_f}{\dot{m}_{H_2}\bullet LHV_{H_2}}\times 100\% \tag{34}$$

Where P_{FC} is the power density of the fuel cell, U_f is the utilization factor and $\dot{m}_{H_2}$ is the molar flowrate of H_2. The current generated by fuel cell can be obtained from the equivalent hydrogen flowrate, as shown below

$$n_{H_2,equivalent}(mol/hr)=\left(\frac{I(A)}{2U_f F(C/mol)}\right)\bullet 3600(s/hr) \tag{35}$$

Where U_f is the fuel utilization factor, F is the Faraday's constant and I represents the current.

The amount of oxygen for cathode can be calculated by the anode hydrogen equivalent molar flowrate and fuel utilization factor, as shown as

$$n_{O_2,\text{required}}(\text{mol/hr}) = (0.5)U_f n_{H_2,\text{equivalent}} \quad (37)$$

As mentioned, the efficiency of SECLR process and fuel cell system are achieved. Then, the efficiency of integrated process can be calculated as shown below

$$\eta_{\text{system}}(\%) = \eta_{\text{SECLR}}\eta_{\text{FC}} \quad (38)$$

6.2 Result and discussion

The purity of H_2 in reformate gas which is used as fuel of HT-PEMFC depend on the operating condition such as feed ratio and reforming temperature. As mention, the optimal operating temperature and suitable amount of solid (NiO and CaO) circulation in the process were indicated in a previous chapter. Therefore, the effect of S/B on HT-PEMFC performance must be investigated because it affects to the H_2 yield, H_2 purity and CO fraction. In addition, the unsuitable composition of reformate gas can reduce the efficiency of this system. Therefore, the effect of S/B ratios on thermal efficiency of SECLR are shown in Table 6.1.

6.2.1 Effect of steam to biogas ratio on the thermal efficiency of SECLR process

As mentioned, a SECLR process operated with high S/B ratio can produce the high amount of hydrogen rich gas and consumes high energy for steam generation.

Therefore, this part shows the thermal efficiency of SECLR process at various S/B ratios. This case is simulated at biogas feed rate 1 kmol/hr, NiO/B ratio of 0.5, CaO/B ratio of 0.85 with reforming temperature 500 °C. There are three case of S/B ratios which are examined in this simulation. Then the values of hydrogen yields are used to determine efficiency of SECLR system. The thermal efficiency calculation of this process is based on using LHV of biogas and hydrogen.

Table 6.1 Thermal efficiency of SECLR process operated with biogas 1 kmol/hr and different S/B ratios at reforming temperature 500 ºC.

Steam-biogas ratio	H_2 yield (kmol/hr)	Thermal efficiency (%)
1	1.36	52.62
1.5	1.40	53.48
2	1.41	53.83

The results in table 6.1 show that the thermal efficiency of SECLR process without heat integration system is increased with increasing the S/B ratio. The SECLR process operated with higher S/B ratio consumes more energy to produce steam for the reforming feed. For these reasons, the heat requirement of the system and amount of hydrogen must be considered to identify suitable operating condition.

Table 6.2 Mole fraction and mole flowrate of hydrogen at different steam to biogas ratio

S/B ratio	Mole fraction of CO	Mole fraction of H_2	Mole flowrate of H_2
1	0.000109	0.874939	1.36
1.5	0.002143	0.884306	1.40
2	0.001756	0.886456	1.41

Three case of fuels which are obtained by varying S/B ratio of 1, 1.5, 2 and reforming temperature 500 ºC are used to determine the HT-PEM performance. They can indicate the performance of HT-PEMFC in a term of S/B ratio. The amount of hydrogen and hydrogen purity affects the cell voltage which is related with electrical power of fuel cell.

The polarization curve illustrate the plot of current density and cell voltage. They can be used to calculate the power output of HT-PEMFC. The characteristic of the HT-PEMFC operated by H_2 from SECLR process at S/B ratio of 2 is shown in Figure 6.1

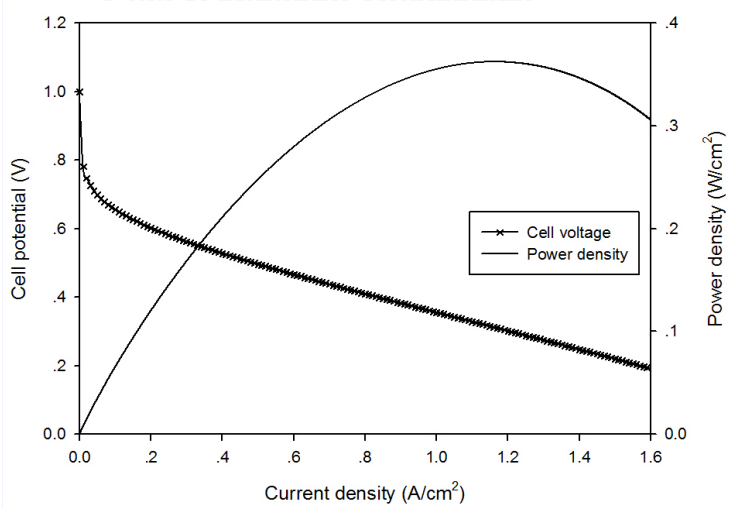

Figure 6.1 Polarization curve and power density of the HT-PEMFC

6.2.2 Effect of utilization factor on the efficiency of HT-PEMFC

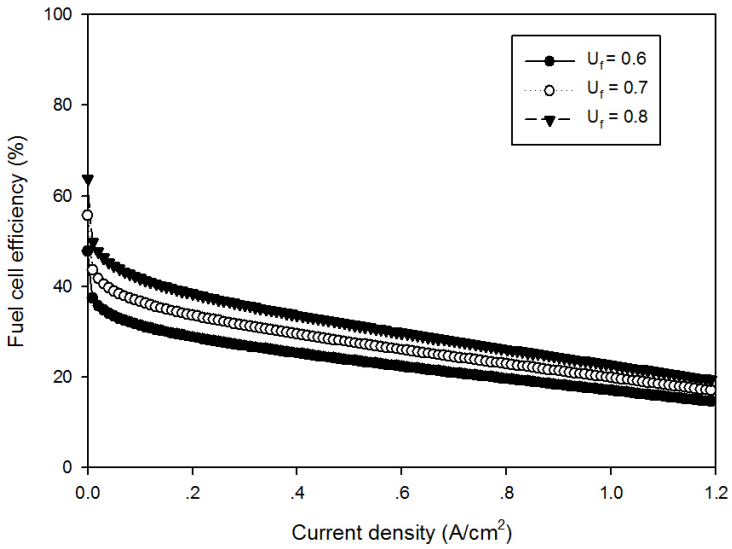

Figure 6.2 Effect of operating current density on fuel cell efficiency with different fuel utilization factor

The effect of fuel utilization on fuel cell efficiency is shown in Figure 6.2. The result show that the high fuel cell efficiency can be obtained at high utilization factor. In contrast, the fuel utilization factor over 0.8 can increase CO concentration that is CO poisoning on Pt catalyst because the concentration of H_2 on catalyst surface is depleted by electrochemical reaction. It is observed that the HT-PEMFC is more efficient at low current density of all fuel utilization factor.

6.2.3 Effect of utilization factor on the heat recovery from HT-PEMFC

The anode off gas which does not react in anode can be separated for using as a fuel in afterburner. The heat generated in afterburner can be recovered to use in reforming process. Therefore, the amount of anode off gas is varied and then used to indicate the amount of heat recovery by fuel utilization. Figure 6.2 shows the heat recovery from fuel cell system with varying the fuel utilization.

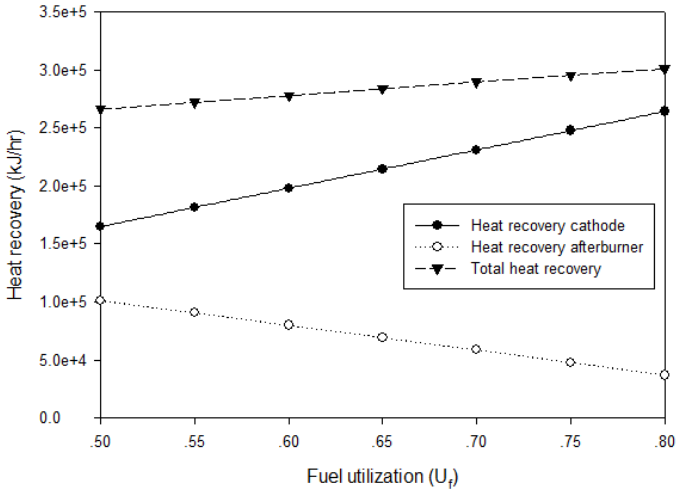

Figure 6.3 Effect of U_f on heat recovery from HT-PEMFC at S/B ratio of 2 and cell temperature 160 ºC.

6.3 Conclusion

In this chapter, it can conclude that the highest thermal efficiency is shown in the SECLR which is operated at S/B ratio of 2 due to high hydrogen yield. In a part of oxygen carrier, the highest thermal efficiency can be obtained at NiO/B of 0.5 because the H_2 yield and purity is decreased by increasing NiO/B ratio due to complete oxidation reduction. In term of fuel cell, the increasing of fuel utilization factor can obtain high HT-PEMFC efficiency at various current densities due to increasing electrical power output. The HT-PEMFC operated at low current density achieves the high efficiency. In real process, the suitable current density should operates at high cell voltage and linear region of polarization curve due to activation and concentration losses avoidance. Therefore, the cell voltage is chosen at 0.6 V for analysis in the next part.

CHAPTER VII

EXERGY ANALYSIS

The use of exergy as a tool for improving the efficiency of SECLR and HT-PEMFC integrated system is described in this chapter. It can be used as indication of what the maximum of work can be achieved. For real process, the energy quality is destroyed by the energy transformation process. In this work, biogas is used as energy resource for the electrical power generation by fuel cell. Thus, exergy analysis is properly tool for system analysis. Moreover, the exergetic loss and destruction of each unit are evaluated and used as data for process improvement. It can indicate that how the process can produce eficiently useful work. Then, the exergy loss and destruction is reduced by heat integration and can reach to the higher exergy efficiency process.

As mentioned, the energy quality or exergy of heat is considered for heat integration in the process. It can use an approach to development the process efficiency. In chemical process, the important term of exergy analysis is chemical exergy because the maximum work can be achieved by taking to equilibrium with constant temperature and pressure with reference environment state. The standard chemicals exergy at reference environment state 25 ºC and 1 atm which are used in this study are shown in Table 7.1.

Table 7.1 The standard chemical exergy of substances.

Substance	**State**	**Standard chemical exergy (kJ/kmol)**
CH_4	Gas	836510
H_2	Gas	238490
CO_2	Gas	20140
CO	Gas	275430
N_2	Gas	720
O_2	Gas	3970
H_2O	liquid	11710
NiO	Solid	38460
Ni	Solid	252800
CaO	Solid	119620
$CaCO_3$	Solid	16300

7.1 Result and discussion

The effect of operating parameters of SECLR process on exergy destruction and efficiency are analyzed. For achieving higher efficiency, the principle of exergy analysis is used to identify defect caused by ineffectiveness exergy consumption and to improve the heat integration in this process. The heat requirement and heat available for each unit are considered for reducing external energy consumption. Figure 7.1 illustrates a schematic of SECLR without heat integration that is used to determine the heat of each unit and stream. Consequently, the key to minimize exergy loss and destruction in the process is studied as shown below.

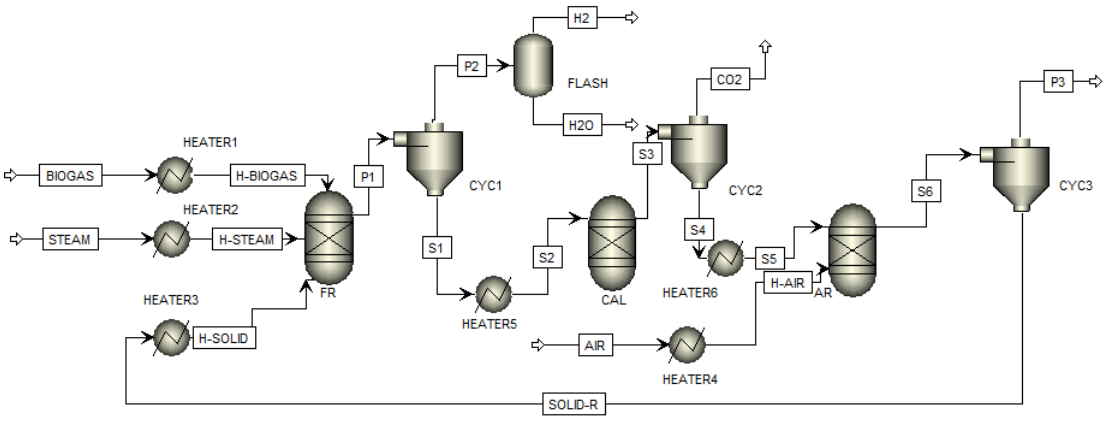

Figure 7.1 A schematic of SECLR process before exergy efficiency improvement

7.1.1 Energy integration analysis

First, the energy integration analysis is the calculation of the minimum heating and cooling requirements for heat-exchanger network. In this process, there are several streams that need to be heated and cooled. The difference between the available heat in the hot streams and the required heat in the cold streams is the net amount of heat that must be supplied or removed. These cold streams are assumed in ambient temperatures of 25 ºC. The parameters and operating condition which are obtained from chapter V are used in energy and exergy analysis. These operating condition are defined as suitable operating condition. They are shown in table 7.2

Table 7.2 Suitable operating conditions for hydrogen production from biogas SECLR process

Parameters	Value
Biogas feed (kmol/hr)	1.0
NiO to biogas ratio (NiO/B)	0.5
Steam to biogas ratio (S/B)	2
Air to biogas ratio (A/B)	4
Calcium oxide to biogas ratio (CaO/B)	0.85
Fuel reactor temperature (ºC)	500
Calcination reactor temperature (ºC)	900
Air reactor temperature (ºC)	1000
Flash drum temperature (ºC)	25
Operating pressure (atm)	1

Table 7.3 shows that the heat available and heat requirement of each stream are calculated by first law of thermodynamic in Aspen Plus software. For heat integration, the heat can be only transferred from a hot stream to a cold stream if the temperature of the hot stream higher than the cold stream. However, this study does not consider only term of energy but the exergy destruction of each unit is determined simultaneously. In exergy analysis, the chemical reactions and heat transfer in a process affect to the rate of exergy destruction. The inefficiencies in a system is caused by the exergy loss and exergy destruction. However, the exergy destruction can be divided into two parts, the avoidable exergy and the unavoidable exergy**.**

The exergy efficiencies can be calculate by a ratio of net exergy output to net exergy input, as shown as below:

$$\psi_{FC}(\%)=\left(\frac{\dot{W}_{FC}}{\dot{n}_{fuel}\bullet\dot{E}x_{fuel}}\right)\times 100 \quad (39)$$

Where ψ_{FC} is exergy efficiency, $\dot{W}_{FC}$ is the electrical power and $\dot{E}x_{fuel}$ is chemical exergy of fuel.

Table 7.3 Descriptions of streams

Stream	Condition	T_{in} (C)	T_{out} (C)	$Q_{available}$ (kJ/hr)
BIOGAS	Cold	25	500	-21143.74
STEAM	Cold	25	500	-121898.01
AIR	Cold	25	1000	- 123849.01
P2	Hot	500	25	114900.60
CO2	Hot	900	25	35919.95
P3	Hot	1000	25	103036.98

In this simulation, all of reactors are operated with isothermal condition. Therefore, the heat of reaction with constant temperature of all reactors can be calculated. The amount of heat requirement, heat available and exergy destruction of each unit are shown in Table 7.4. For exergy efficiency improvement, the exergy balance of each reactor is determined and then the results of exergy balance can indicate the location of exergy destruction. Therefore, the aim of this section is to find the avoidable exergy destruction for improvement. The exergy balance can be divided in three components, such as exergy of heat, physical exergy and chemical exergy. Then, they are used to compute the destroyed exergy rate due to irreversible process. The total exergy change is evaluated by the transfer of energy by the heat and work of the process.

Table 7.4 Heat duty and exergy destruction of each unit.

Unit	T	Heat duty (kJ/hr)	Ex_d (kJ/hr)
Fuel reactor (FR)	500	-76190.53	123,357.86
Calcination reactor (CAL)	900	143825.84	7,679.00
Air reactor (AR)	1000	-122841.24	203,537.74
Flash (FLASH)	25	-114900.58	23,033.14
Heater 1 (HEATER1)	500	21143.74	4,090.11
Heater 2 (HEATER2)	500	121898.01	43,894.27
Heater 3 (HEATER3)	500	33358.54	5,500.35
Heater 4 (HEATER4)	1000	123849.01	24,858.14
Heater 5 (HEATER5)	900	52002.39	3,128.48
Heater 6 (HEATER6)	1000	8192.45	83.88
Total			439,162.97

From these results, the magnitude of exergy destruction is occurred in the air reactor. The fuel reactor or reforming reactor which is the highly exergy destruction is the same as air reactor. The exothermic reactors are the main of exergy destruction in a process because the heat released from these reactors do not use properly. In contrast, the calcination reactor and heaters which require heat to supply are not high exergy destruction. For these reason, these data are primary used for reducing exergy destruction by heat integration. Therefore, the exergy analysis is employed for the process improvement. For heat integration, a term of exergy of heat shows that the heat must be transferred with low temperature gradient to decrease the exergy destruction caused by exergy of heat.

7.1.2 Effect of steam to biogas ratio on exergy destruction of SECLR process

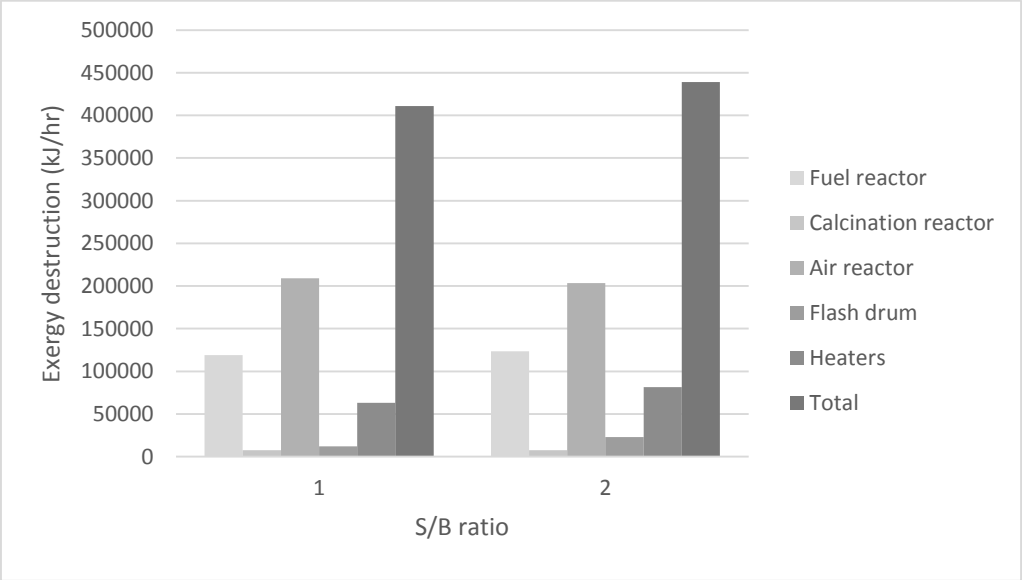

Figure 7.2 A comparison of exergy destruction of SECLR process operated with S/B ratios of 1 and 2

Figure 7.2 illustrated the comparison of exergy destruction of each unit between SECLR process operated with S/B ratio of 1 and 2. The result show that the total exergy destruction of SECLR which is operated with S/B ratio of 2 is higher than S/B of 1 due to heat requirement of steam generation. However, SECLR which operates at S/B ratio of 2 can be obtained higher hydrogen yield. Therefore, the exergy efficiency must be considered. Then, the results show that the exergy efficiency of SECLR operated with S/B ratio of 2 obtains at 53.21% that is lower than S/B ratio of 1 which exergy efficiency is 55.00%.

7.1.3 Effect of NiO to biogas ratio on exergy destruction and heat recovery from air reactor of SECLR process

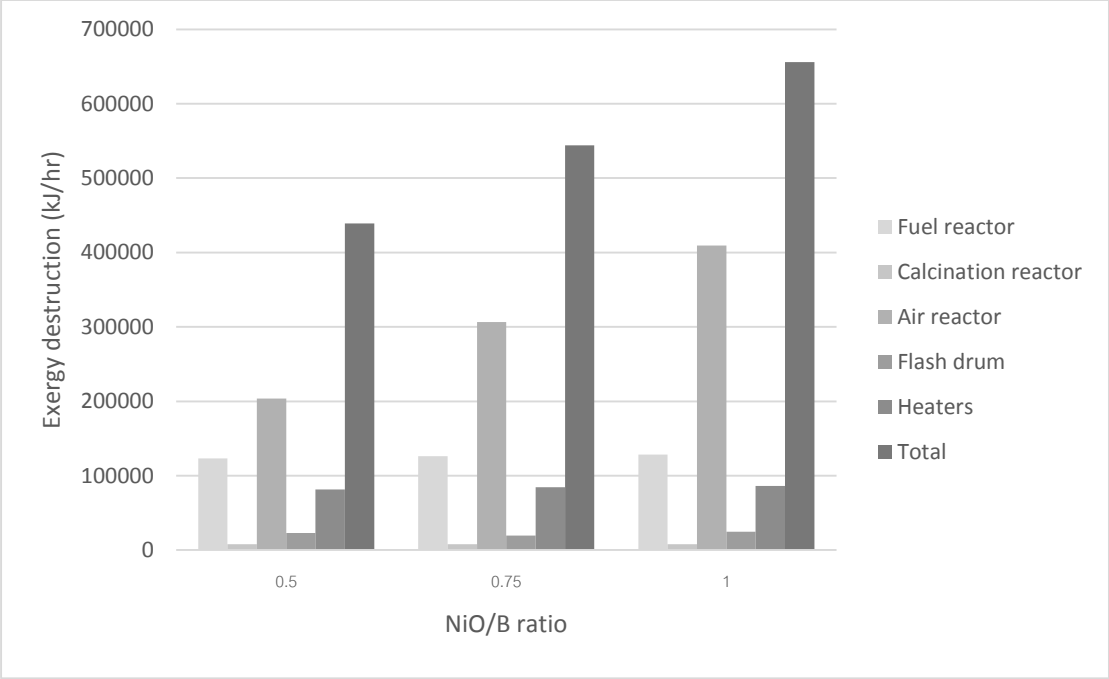

Figure 7.3 Exergy destruction of each unit with different NiO/B ratio

In term of metal oxide in SECLR process, the initial NiO/B ratio is analyzed at 0.5. In Figure 7.3, the effect of NiO on exergy destruction of each unit is investigated at biogas 1 kmol/hr, S/B ratio of 2, CaO/B ratio of 0.85 and reforming temperature at 500 °C. The results show that the increasing of NiO/B ratio increases exergy destruction of fuel reactor, air reactor and all solid heaters. As mentioned, NiO is well known that it can be used as oxygen carrier and energy carrier. Therefore, the air reactor which is used as both NiO regenerator and heat source for system is considered. In addition, the effect of NiO/B on the hydrogen yield that the increasing of NiO/B ratio decreases the amount of hydrogen. Therefore, the amount of heat recoverable which obtain form air reactor and energy carrier as NiO are calculated. In term of heat recovery calculation,

air reactor is operated at Air/B ratio of 4 and temperature 1000 °C. Figure 7.4 shows that the heat recovery of each unit is increased with increasing amount of NiO.

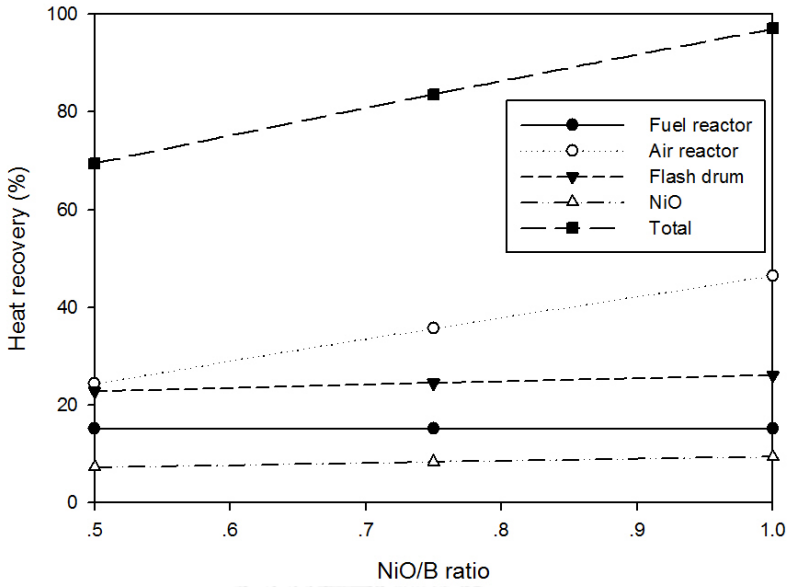

Figure 7.4 Heat recovery of SECLR process at various NiO/B ratios

Although the heat recovery of this system depends on the amount of NiO, hydrogen yield decreases with increasing of NiO due to complete oxidation reactions. The quality of process must be considered. Then, the exergy efficiency of system with different NiO/B ratio is analyzed. The result of exergy efficiency with varying NiO/B ratios is shown in Figure 7.5. The exergy efficiency obtainable at NiO/B ratios of 0.5, 0.75, and 1 are 53.21%, 48.06% and 40.82%, respectively.

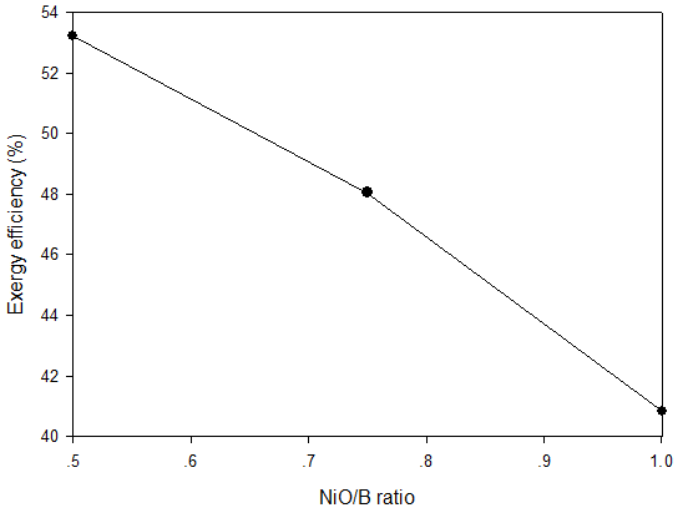

Figure 7.5 The exergy efficiency of SECLR process at various NiO/B ratio**.**

7.1.4 Effect of cell temperature on exergy destruction and exergy efficiency

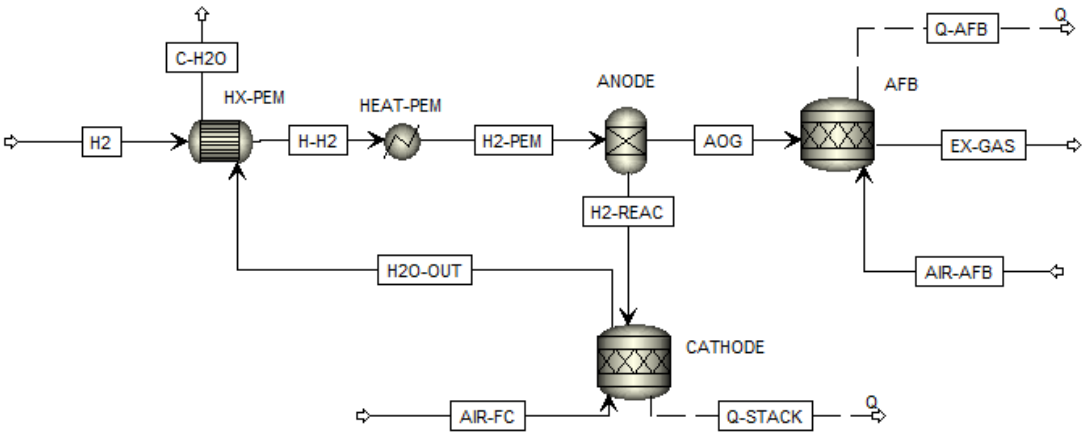

Figure 7.6 A schematic of a HT-PEMFC using in this system

HT-PEMFC is a main point of this study. It is used to produce electric power and heat to supply the heat-required for unit. For these reason, the characteristic of HT-PEMFC is analyzed by operating parameter. The variation of exergy efficiency and exergy destruction depend on different operating conditions such as cell temperature, current density. As mentioned, HT-PEMFC operated at different current density can

affect to the exergy efficiency due to changing of heat recovery rate. Table 7.5 shows that the exergy destruction of each units which are used for HT-PEMFC stack simulation are operated by feed H_2 1.41 kmol/hr with different temperature and afterburner is fixed temperature 1000 ºC. The result shows that the exergy destruction of HT-PEMFC increase with increasing cell temperature due to higher heat energy requirements for system.

Table 7.5 Exergy destruction of each unit using in HT-PEMFC simulation

Process Unit	Ex_d (150 ºC) (kJ/hr)	Ex_d (160 ºC) (kJ/hr)	Ex_d (170 ºC) (kJ/hr)
HX-PEM	474.49	539.05	2933.01
HEAT-PEM	0.05	0.05	0.05
HT-PEMFC	357382.77	361729.48	365620.17
AFB	53939.85	54066.01	54194.17
Total	411797.20	416334.60	422747.40

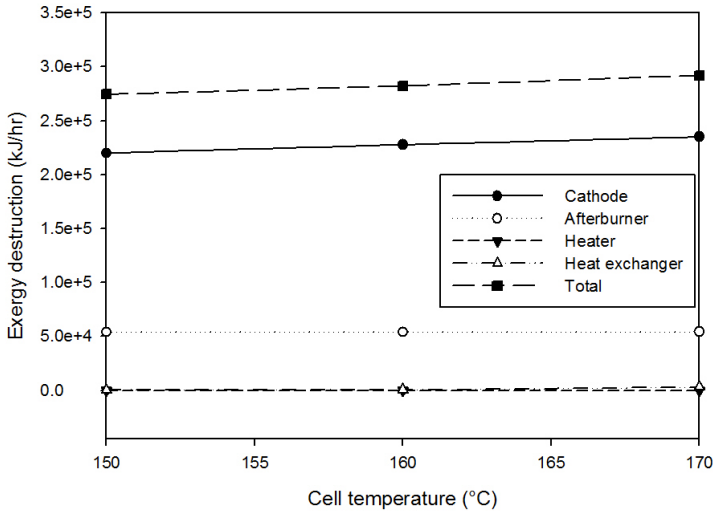

Figure 7.7 Exergy destruction of fuel cell at different cell temperature

7.1.5 Effect of operating current density on exergy destruction and exergy efficiency

The effect of operating current density on exergy destruction and exergy efficiency of HT-PEMFC are studied in this part. It is operated at utilization factor 0.8. The effect of current density on exergy efficiency of HT-PEMFC are shown in Figure 7.8. The result shows that the exergy efficiency of HT-PEMFC is reduced by operating with high current density because the voltage loss of HT-PEMFC occurs rapidly with respect to increasing current density and decreases the output power of fuel cell. Then the efficiency of fuel cell is reduced with high current density due to irreversible loss such as electrode activation loss, ohmic loss and concentration loss. At high current density, the concentration loss is increased by mass transfer limitation. In term of fuel cell temperature, the higher fuel cell temperature increases exergy destruction due to increasing rate of electrochemical reaction.

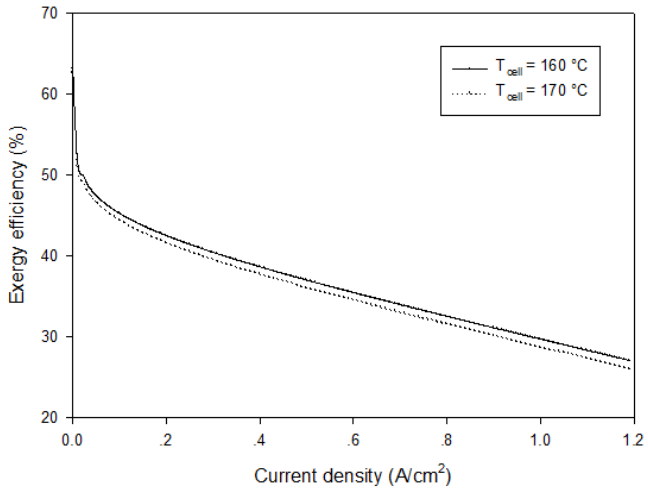

Figure 7.8 Effect of operating current density on exergy efficiency with different temperature.

The effect of S/B ratio on exergy efficiency of system which is carried out with varying current densities is investigated. The result shows that the increasing of S/B ratio can improve exergy efficiency of system because the high hydrogen yield is obtained at the high S/B ratio, as shown in Figure 7.9. Then, it can increase the electrical power output and obtain heat recovery from cathode and afterburner which hydrogen is used as fuel.

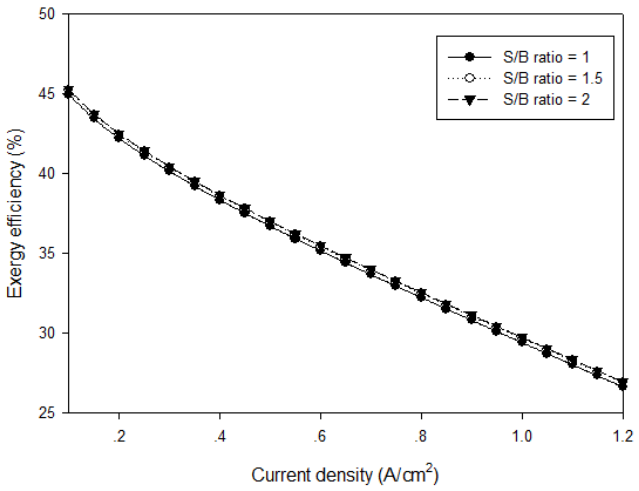

Figure 7.9 Effect of S/B ratio on exergy efficiency with different cell temperature

7.1.6 Process improvement using exergy analysis

In this section, HT-PEMFC is integrated with SECLR process. The heat produced by cathode of fuel cell can be used to preheat the reactants. The afterburner operated at 1000 ºC is used to generate heat to supply the heater which is used to preheat air that is used in air reactor. The heat exchanger is employed to transfer thermal energy between products and reactants. Firstly, it is found that the heat available from air reactor can properly supply to calcination reactor. Then, the exergy destruction of air reactor can be decreased.

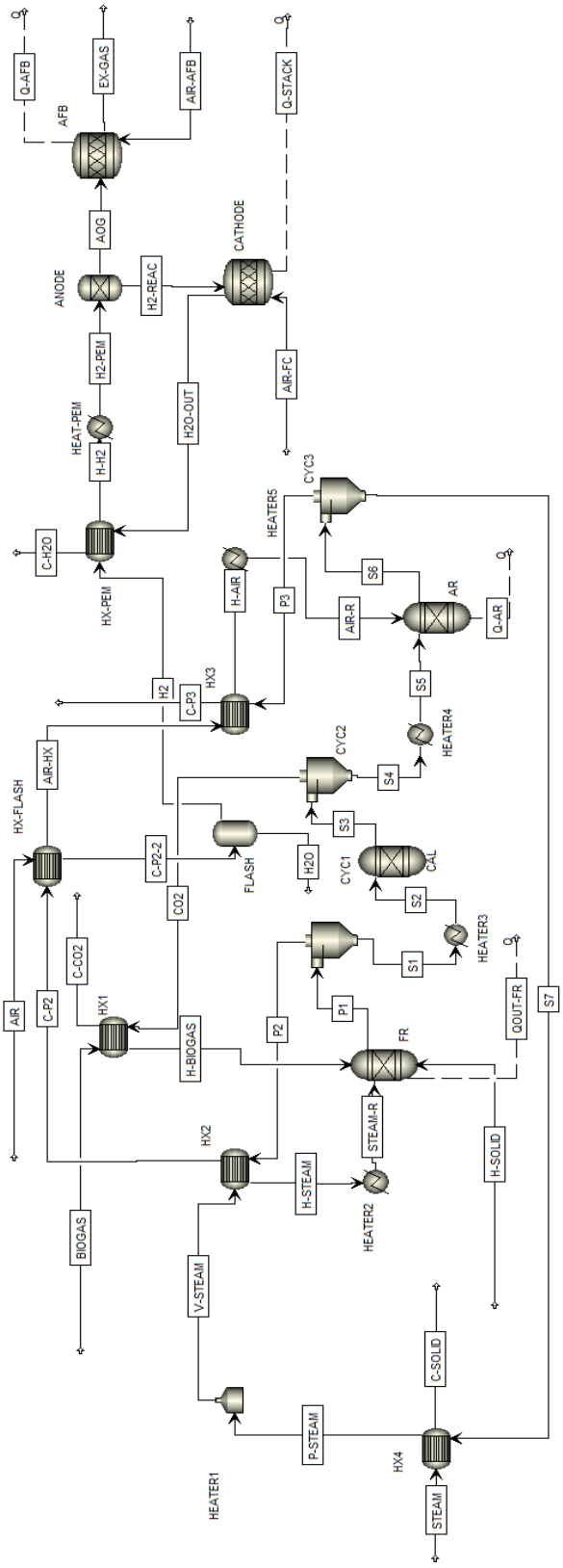

Figure 7.10 A schematic of SECLR and HT-PEMFC integrated system

Table 7.6 Exergy analysis of each unit process.

Unit	**Ex_{in} (kJ/hr)**	**Ex_{out}(kJ/hr)**	**Ex_{d}(kJ/hr)**	**Ex_{loss}(kJ/hr)**
FR	660,993.66	537,644.88	123,348.78	-
CAL	302,212.10	294,699.20	7512.90	11,979.53
AR	334,480.00	223,772.90	110757	-
FLASH	363,312.37	360,381.53	2930.84	-
HEATER1	23,699.07	17,783.08	5915.99	70,141.83
HEATER2	31,010.83	31,010.72	0.11	-
HEATER3	58,914.46	56,053.76	2860.70	-
HEATER4	38,289.62	38,189.74	99.88	-
HEATER5	70,049.77	69,998.72	51.05	-
HX1	19,900.55	14,516.20	5384.35	-
HX2	45,617.38	43,893.30	1724.08	-
HX3	69,816.30	68,418.40	1397.90	-
HX4	39,135.43	14,834.05	24301.38	-
HXFLASH	12,929.63	12,129.38	800.24	-
HX-PEM	360,091.70	359,552.65	539.05	-
HEAT-PEM	343,627.42	343,627.37	0.05	-
ANODE	-	-	-	-
CATHODE	379,298.56	165,763.27	121,819.10	-
AFB	53,239.19	19,602.47	33636.72	-
Total	3,206,618.04	2,671,871.62	443,080.12	82,121.36

From Table 7.6, the integrated system is fed by biogas 1 kmol/hr and HT-PEMFC is operated at cell temperature 160 ºC and cell voltage 0.6 V. The simulation is used to analyze the exergy destruction of each unit. The results show that the majority of exergy destruction is occurred by reforming reactor or fuel reactor. The exergy destruction of reforming reactor is caused by the many reactions which are irreversible reactions. The cathode side of HT-PEMFC is the second of exergy destruction because the hydrogen which has high chemical exergy is converted to water by electrochemical reaction. However, the cathode side where is used to generate the electricity and heat as by-product. This integrated system can produce electricity 82,121.36 kJ/hr. In this process, the heat of cathode that is used to preheat steam for the fuel reactor. In term of exergy of heat, the exergy destruction of fuel reactor can be reduced by using heat release of reforming reactor.

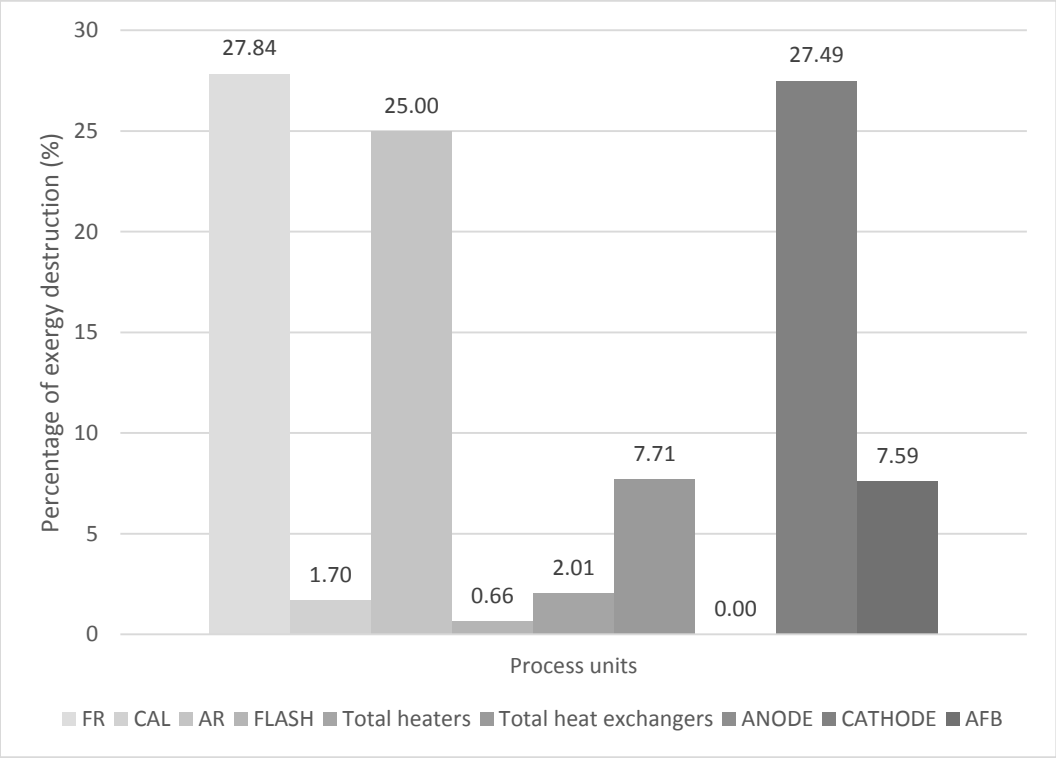

Figure 7.11 Percentage of exergy destruction of each unit.

In this case study, the exergy destruction of each unit in process which is improved by using exergy analysis shows the result in Table 7.6. It can be seen that the total of exergy destruction of this process is reduced from 859,414.72 kJ/hr to 443,080.12 kJ/hr. These results are obtain by total exergy balance of each unit. However, there are exergy losses which is related to exergy of heat across the units. The result shows the total exergy loss is 100,478.30 kJ/hr. The exergy efficiency of SECLR process that is improved by heat integration obtain the exergy efficiency at 63.03 % which is higher than before process at 53.21%, as shown in Table 7.7. The comparison of thermal efficiency and exergy efficiency of the global system are 41.98% and 26.72%, respectively. It can be observed that the exergy efficiency is lower than thermal efficiency due to the influence of exergy destruction and exergy loss in the system.

Table 7.7 Comparison of exergy efficiency and thermal efficiency of this system

Process	η_{Thermal} (%)	η_{Exergy} (%)
SECLR	67.15	63.03
HT-PEMFC	62.52	42.40
Global system	41.98	26.72

7.2 Conclusion

In this chapter, the performance of SECLR process and HT-PEMFC are analyzed by varying operating parameters such as S/B ratios, NiO/B ratios, fuel cell temperatures, operating current densities. The results indicate that S/B ratio of 2 can achieve the highest efficiency of system. Although the heat consumption of process which is operated by S/B ratio of 2 is higher, it can produce more hydrogen yield.

Therefore, the higher net power output of the system can be obtained. In the next section, the effect of NiO/B ratio on system efficiency is investigated by the calculation of net power input and hydrogen yield. It can be observed that the increasing of NiO/B ratio decreases the hydrogen yield. However, the higher heat recovery of the system is obtained at high NiO/B ratio.

The last section shows that the exergy analysis of SECLR, HT-PEMFC and integrated system are analyzed. The exergy destruction of each unit is calculate. The air reactor is the highest exergy destruction and the fuel reactor is the second. These data are used to the process improvement by heat integration. After heat integration, the result shows that the exergy destruction of process is reduced and the higher exergy efficiency of the process is obtained in this work.

CHAPTER VIII

CONCLUSION AND RECOMMENDATION

8.1 Conclusion

The purpose of this study is the simulation and parameters sensitivity analysis of sorption enhance chemical looping reforming processor integrated with HT-PEMFCs system. Both of the simulations are good agreement with the experimental data. The simulations show that the effect of parameters on performance of SECLR and HT-PEMFC such as S/B, NiO/B, CaO/B, reforming temperature, and operating current density. The fuel utilization factor of fuel cell which amount of hydrogen is consumed by electrochemical is varied. It can be used to investigate energy balance of the system and electrical power output. Then, the results can identify the suitable operating condition for the system and is used to improve performance of the system.

In addition, the energy management in a process must be considered to provide high efficiency system. Exergy can provide a much better understanding of this process. It is used to determine exergy destructions and exergy losses. Therefore, the exergy analysis can indicate the exergy efficiency which relates to the quality of energy in this process. The quality of energy using for heat integration is shown in term of exergy loss between units. This research shows the parameters which influences on the thermal efficiency and exergy efficiency. Finally, they used to improve process by heat integration to reduce exergy destruction in the system and then, the higher exergy efficiency system is obtained in this work.

8.2 Recommendation

This research is the elementary exergy analysis of a SECLR process integrated with HT-PEMFC which is steady state model and thermodynamic calculation. In addition, the sensitivity analysis is only the elementary calculation due to many assumptions. Therefore, the future works should be analyzed close to the real process behavior which should use dynamic model and kinetic model. Moreover, this operating conditions should be optimized by minimizing the exergy destruction.

REFERENCES

Adanez, J., Abad, A., Garcia-Labiano, F., Gayan, P., and Luis, F. (2012). Progress in chemical-looping combustion and reforming technologies. *Progress in Energy and Combustion Science,* 38(2), 215-282.

Al Seadi, T. (2008). *Biogas handbook*: Syddansk Universitet.

Amphlett, J., Mann, R., and Peppley, B. (1996). On board hydrogen purification for steam reformation/PEM fuel cell vehicle power plants. *International Journal of Hydrogen Energy,* 21(8), 673-678.

Araki, S., Hino, N., Mori, T., and Hikazudani, S. (2010). Autothermal reforming of biogas over a monolithic catalyst. *Journal of Natural Gas Chemistry,* 19(5), 477-481.

Araya, S. S., Andreasen, S. J., Nielsen, H. V., and Kær, S. K. (2012). Investigating the effects of methanol-water vapor mixture on a PBI-based high temperature PEM fuel cell. *International Journal of Hydrogen Energy,* 37(23), 18231-18242.

Avraam, D., Halkides, T., Liguras, D., Bereketidou, O., and Goula, M. (2010). An experimental and theoretical approach for the biogas steam reforming reaction. *International Journal of Hydrogen Energy,* 35(18), 9818-9827.

Barbir, F. (2012). *PEM fuel cells: theory and practice*: Academic Press.

Benziger, J., Nehlsen, J., Blackwell, D., Brennan, T., and Itescu, J. (2005). Water flow in the gas diffusion layer of PEM fuel cells. *Journal of Membrane Science,* 261(1), 98-106.

Braga, L. B., Silveira, J. L., Da Silva, M. E., Tuna, C. E., Machin, E. B., and Pedroso, D. T. (2013). Hydrogen production by biogas steam reforming: A technical, economic and ecological analysis. *Renewable and Sustainable Energy Reviews,* 28, 166-173.

Chattanathan, S. A., Adhikari, S., McVey, M., and Fasina, O. (2014). Hydrogen production from biogas reforming and the effect of H_2S on CH_4 conversion. *International Journal of Hydrogen Energy,* 39(35), 19905-19911.

Cheddie, D., and Munroe, N. (2006). Mathematical model of a PEMFC using a PBI membrane. *Energy Conversion and Management,* 47(11), 1490-1504.

da Silva, A. L., Dick, L. F. P., and Müller, I. L. (2012). Performance of a PEMFC system integrated with a biogas chemical looping reforming processor: a theoretical analysis and comparison with other fuel processors (steam reforming, partial oxidation and auto-thermal reforming). *International Journal of Hydrogen Energy,* 37(8), 6580-6600.

Dieter, H., Bidwe, A. R., Varela-Duelli, G., Charitos, A., Hawthorne, C., and Scheffknecht, G. (2014). Development of the calcium looping CO_2 capture technology from lab to pilot scale at IFK, University of Stuttgart. *Fuel*, 127, 23-37.

Dimopoulos, G. G., Stefanatos, I. C., and Kakalis, N. M. (2013). Exergy analysis and optimisation of a steam methane pre-reforming system. *Energy*, 58, 17-27.

Dincer, I., and Rosen, M. A. (2012). *Exergy: energy, environment and sustainable development*: Newnes.

Dou, B., Song, Y., Wang, C., Chen, H., Yang, M., and Xu, Y. (2014). Hydrogen production by enhanced-sorption chemical looping steam reforming of glycerol in moving-bed reactors. *Applied Energy*, 130, 342-349.

Effendi, A., Hellgardt, K., Zhang, Z.-G., and Yoshida, T. (2005). Optimising H_2 production from model biogas via combined steam reforming and CO shift reactions. *Fuel*, 84(7), 869-874.

Gopaul, S. G., and Dutta, A. (2015). Dry reforming of multiple biogas types for syngas production simulated using Aspen Plus: The use of partial oxidation and hydrogen combustion to achieve thermo-neutrality. *International Journal of Hydrogen Energy*, 40(19), 6307-6318.

Gou, B., Na, W., and Diong, B. (2009). *Fuel cells: modeling, control, and applications*: CRC press.

Hajjaji, N., Baccar, I., and Pons, M.-N. (2014). Energy and exergy analysis as tools for optimization of hydrogen production by glycerol autothermal reforming. *Renewable Energy*, 71, 368-380.

Hajjaji, N., Pons, M.-N., Houas, A., and Renaudin, V. (2012). Exergy analysis: An efficient tool for understanding and improving hydrogen production via the steam methane reforming process. *Energy Policy*, 42, 392-399.

Herdem, M. S., Farhad, S., and Hamdullahpur, F. (2015). Modeling and parametric study of a methanol reformate gas-fueled HT-PEMFC system for portable power generation applications. *Energy Conversion and Management*, 101, 19-29.

Herout, M., Malaťák, J., Kučera, L., and Dlabaja, T. (2011). Biogas composition depending on the type of plant biomass used. *Research in Agricultural Engineering*, 57(4), 137-143.

Jiang, Z., and Jiang, Z.-J. (2011). *Carbon Nanotubes Supported Metal Nanoparticles for the Applications in Proton Exchange Membrane Fuel Cells (PEMFCs)*: INTECH Open Access Publisher.

Klinedinst, K., Bett, J., Macdonald, J., and Stonehart, P. (1974). Oxygen solubility and diffusivity in hot concentrated H 3 PO 4. *Journal of Electroanalytical Chemistry and Interfacial Electrochemistry,* 57(3), 281-289.

Mamlouk, M., Sousa, T., & Scott, K. (2010). A high temperature polymer electrolyte membrane fuel cell model for reformate gas. *International Journal of Electrochemistry*, 2011.

Mukherjee, S., Kumar, P., Yang, A., and Fennell, P. (2015). Energy and exergy analysis of chemical looping combustion technology and comparison with pre-combustion and oxy-fuel combustion technologies for CO2 capture. *Journal of Environmental Chemical Engineering,* 3(3), 2104-2114. doi: http://dx.doi.org/10.1016/j.jece.2015.07.018

Nalbandian, L., Evdou, A., and Zaspalis, V. (2011). La 1− x Sr x M y Fe 1− y O 3− δ perovskites as oxygen-carrier materials for chemical-looping reforming. *International Journal of Hydrogen Energy,* 36(11), 6657-6670.

Obara, S. y., Tanno, I., Kito, S., Hoshi, A., and Sasaki, S. (2008). Exergy analysis of the woody biomass Stirling engine and PEM-FC combined system with exhaust heat reforming. *International Journal of Hydrogen Energy,* 33(9), 2289-2299.

Pariphat Chungchaichana, S. V. (2012). Potential analysis of fresh-food market waste for biogas production to electricity ; case study Talad-Thai. วารสารวิจัยพลังงาน.

Pimenidou, P., Rickett, G., Dupont, V., and Twigg, M. V. (2010). High purity H_2 by sorption-enhanced chemical looping reforming of waste cooking oil in a packed bed reactor. *Bioresource technology,* 101(23), 9279-9286.

Rydén, M., Lyngfelt, A., and Mattisson, T. (2006). Synthesis gas generation by chemical-looping reforming in a continuously operating laboratory reactor. *Fuel,* 85(12), 1631-1641.

Rydén, M., and Ramos, P. (2012). H 2 production with CO_2 capture by sorption enhanced chemical-looping reforming using NiO as oxygen carrier and CaO as CO 2 sorbent. *Fuel Processing Technology,* 96, 27-36.

Scott, K., and Mamlouk, M. (2009). A cell voltage equation for an intermediate temperature proton exchange membrane fuel cell. *International Journal of Hydrogen Energy*, 34(22), 9195-9202.

Shamardina, O., Chertovich, A., Kulikovsky, A., and Khokhlov, A. (2010). A simple model of a high temperature PEM fuel cell. *International Journal of Hydrogen Energy,* 35(18), 9954-9962.

Simpson, A. P., and Lutz, A. E. (2007). Exergy analysis of hydrogen production via steam methane reforming. *International Journal of Hydrogen Energy,* 32(18), 4811-4820.

Slattery, J. C., and Bird, R. B. (1958). Calculation of the diffusion coefficient of dilute gases and of the self-diffusion coefficient of dense gases. *AIChE Journal,* 4(2), 137-142.

Spiegel, C. (2008). *Mathematical modeling of polymer exchange membrane fuel cells.* University of South Florida.

Wang, D., Chen, S., Xu, C., and Xiang, W. (2013). Energy and exergy analysis of a new hydrogen-fueled power plant based on calcium looping process. *International Journal of Hydrogen Energy,* 38(13), 5389-5400.

Wang, R., and Rohr, D. (2002). *Natural gas processing technologies for large scale solid oxide fuel cells.* Paper presented at the ABSTRACTS OF PAPERS OF THE AMERICAN CHEMICAL SOCIETY.

Welaya, Y. M., El Gohary, M. M., and Ammar, N. R. (2012). Steam and partial oxidation reforming options for hydrogen production from fossil fuels for PEM fuel cells. *Alexandria Engineering Journal,* 51(2), 69-75.

Zhang, J., Wu, J., and Zhang, H. (2013). *PEM fuel cell testing and diagnosis*: Newnes.

Zhu, X., Li, K., Liu, J.-L., Li, X.-S., and Zhu, A.-M. (2014). Effect of CO 2/CH 4 ratio on biogas reforming with added O_2 through an unique spark-shade plasma. *International Journal of Hydrogen Energy,* 39(25), 13902-13908.

VITA

Mr. Sarunyou Kasemanand was born on October 31, 1991, in Bangkok Thailand. He finished high school from Debsirin in 2010. He received his Bachelor's Degree in Chemical Engineering (second class honors) from Srinakharinwirot University in 2014. He subsequently continued studying the Master of Engineering in Chemical Engineering at the Graduate School of Chulalongkorn University. He has been studying Master's Degree of Chemical Engineer in 2016.